EVALUATION OF MAGNESIUM AS A HALL THRUSTER PROPELLANT

By

Mark A. Hopkins

A DISSERTATION

Submitted in partial fulfillment of the requirements for the degree of

DOCTOR OF PHILOSPHY

In Mechanical Engineering–Engineering Mechanics

MICHIGAN TECHNOLOGICAL UNIVERSITY

This dissertation has been approved in partial fulfillment of the requirements for the Degree of DOCTOR OF PHILOSOPHY in Mechanical Engineering – Engineering Mechanics.

Department of Mechanical Engineering – Engineering Mechanics

Dissertation Advisor:	*Lyon B. King*
Committee Member:	*David Byers*
Committee Member:	*Richard R. Hofer*
Committee Member:	*Bryan H. Suits*
Committee Member:	*Petra Huentemeyer*
Department Chair:	*William W. Predebon*

“Discovery is seeing what everybody else has seen, and thinking what nobody else has thought.”

- Albert Szent-Gyorgyi

Table of Contents

Table of Contents vii

Preface x

Acknowledgements xi

Abstract xiv

Chapter 1 Introduction 16

1.1. Introduction and Motivation 16

1.2. Goal of Research 18

1.3. Structure of Document 20

Chapter 2 Background 22

2.1. Why Magnesium Propellant? 22

2.2. Hall Thrusters 29

2.3. Facility Effects 33

2.4. Condensable Propellant Hall Thrusters 35

Chapter 3 Thermal Mass Flow Control 42

3.1. Goal of Experiment 43

3.2. Experimental Setup and Description of Apparatus 43

3.3. Feasibility Test 46

3.4. Automated Control Tests 50

3.5. Thrust Data 54

3.6. Conclusion 57

Chapter 4 Performance Comparison between a Magnesium- and Xenon-fueled 2 kW Hall Thruster 59

4.1. Goal of Study 59

4.2. Description of Apparatus/Experimental Methods 60

4.3. Measuring the Mass Flow Rate of Magnesium 62

4.4. Magnesium Performance 65

4.5. Xenon Performance 71

4.6. Comparison of Magnesium to Xenon Performance and Discussion of Results 72

4.7. Conclusion 73

Chapter 5 Magnesium Plume Properties and Comparison to Plasma Plumes from Other Propellants 75

5.1. Goal of Study 76

5.2. Description of Apparatus/Experimental Methods 77

5.3. Magnesium and Xenon Plasma Plume Properties at Matched Operating Conditions 79

5.3.1. Plasma Properties—Density, Temperature, and Potential 80

5.3.2. Ion Energy 83

5.3.3. Off-axis Current Distribution 84

5.4. Comparing the Plume Properties of Magnesium and Xenon to Krypton and Bismuth 86

5.5. Discussion 88

5.6. Conclusion 94

Chapter 6 Conclusions/Direction of Future Work 97

6.1. Thermal Mass Flow Control 97

6.2. Performance of the BPT 2000 using Magnesium Propellant 98

6.3. Properties of the Magnesium Plasma Plume and Implications on Thruster Design 99

6.4. Overall Conclusions and Future Work 100

Appendix A. Facility Pressure during Magnesium Thruster Operation 102

Appendix B. Modifying a 5 kW Thruster for Operation using Magnesium 108

References 113

Preface

The majority of Chapter 3 appears in the publication: "Magnesium Hall Thruster with Active Thermal Mass Flow Control," Journal of Propulsion and Power, 30, 2014, pp. 637-644, by Mark A Hopkins and Lyon B. King. Copyright retained by Mark A. Hopkins. In the publication Lyon B. King motivated the research, guided the experimental design, and participated in preparation of the manuscript. Mark A. Hopkins designed and performed the experiments, processed the data, and participated in preparation of the manuscript.

The contents of Chapter 4 have also been submitted in an article for publication in the AIAA Journal of Propulsion and Power coauthored by Mark A. Hopkins and Lyon B. King. In the publication Lyon B. King motivated the research, guided the experimental design, and participated in preparation of the manuscript. Mark A. Hopkins designed and performed the experiments, processed the data, and participated in preparation of the manuscript.

Acknowledgements

Graduate school has been the experience of a lifetime. I've learned more than I ever could have imagined, I've made lifelong friends, and I've made a lot of green plasma—a lot. For each misstep, each challenge, each all-night marathon test there were always people willing to jump in and help. Now that the novel about my graduate research is written, it is time to acknowledge all those people who took the time to help along the way. Below, I have mentioned by name those whose help I could remember at the time I wrote this section. So many people have helped me throughout the years that I am sure I have missed some. Thank you everyone for your help and support.

First, I would like to thank my advisor and my committee. Brad, your enthusiasm as a researcher and guidance as a mentor have been invaluable throughout the course of graduate school. It has been an honor and a pleasure to have had the opportunity to work with you these last seven years. Thank you. To my committee, Dr. Rich Hofer, Dave Byers, Prof. Brian Suits, and Prof. Petra Huentemeyer, I appreciate you taking the time to offer your expertise and advice over the years. Rich, thank you for advice in thruster operation, diagnostics, and design. Dave, thank you for offering your extensive knowledge of condensable propellants and electric propulsion over the years and for taking the time at each conference to guide my research efforts. Professor Suits, your help and advice—starting with your electronics class—have also been invaluable in my education and career trajectory. I met Professor Heuntemeyer late in my education, and

she graciously agreed to be on my committee. Thank you, Dr. Huentemeyer, for taking the time to offer me help and advice.

Research is not possible without funding. I would like to thank the National Science Foundation Graduate Research Fellowship Program for supporting me as a graduate student for the last few years. It is an honor to be among the ranks of such a prestigious group.

To all of my colleagues from the Isp lab who started before me. Dean, thank you for introducing me to the Isp lab and paving the way for the magnesium thruster. Who would have thought underwater hockey would have led to this? Jason Makela, I owe you thanks for far too many things to list them all here. You were the first to welcome me into the lab and show me the ropes. Thank you for taking me under your wing both in and out of the lab; it's an honor to call you my friend. Jason Somerville, thank you for all of the help with coding over the years. When I started, watching me code was like watching a cat bat at string; thank you for your patience. Rob, thank you for the physics lessons and for helping with dozens of thruster tests. Sharing the lab with you for four years was a privilege.

Next thank I want to thank those in my cohort. First I want to thank Aaron. We started rough—you know, with the hissing and whatnot. Thank you for help with electronics and machining over the years and for eventually accepting me as a friend. Next on the list is EJ. We have spent many a late night followed by an early morning in the lab together, and I would do it all over again. Thank you for, shall we say, critiquing (aka slashing and burning) so many of my ideas. On to the Ginger, aka $\sqrt{G^2}$, aka Kurt. You are an excellent friend and coworker. It has been a pleasure to share a lab with you

for the last 4.5 years. Finally Brandon and Amanda, I wish you both the best of luck with your PhDs. Enjoy the experience!

A number of acknowledgments must also go out to faculty and staff at Michigan Tech. My sincerest thanks (and sometimes apologies) go to Master Machinist, Marty Toth. The number of crazy things that you have machined for me is uncountable—peaking with drilling and threading boron nitride ceramic tubes. Thank you. Next my thanks go to Jodi Lehman. Thank you, Jodi, for reading and editing so many of my essays and for your workshops on applying for fellowships. Finally I need to thank the amazing help from the graduate school. Thank you, Dr. Deb Charlesworth, for dealing with all of my incessant questions regarding processes and procedures. You answered all of my questions (sometimes more than once) without even a hint of the irritation I probably deserved.

And of course I want to thank my family: my mom, my dad, and my brothers. Thank you for supporting me through this entire process. I know that choosing a college in the frozen tundra made visiting difficult, so I appreciate the time I did get when you all visited. Thank you to my Houghton family who have dealt with my green plasma stories and never-ending propulsion analogies, thank you for putting up with my nerdiness and supporting me for all these years. Without your support and distractions from my research woes I never would have made it.

Finally thank you, Danny. Many an evening has consisted of me eating dinner and immediately burying my face in a computer until or beyond bedtime. Thank you for your patience and support. I love you.

Abstract

In this study, the use of magnesium as a Hall thruster propellant was evaluated. A xenon Hall thruster was modified such that magnesium propellant could be loaded into the anode and use waste heat from the thruster discharge to drive the propellant vaporization. A control scheme was developed, which allowed for precise control of the mass flow rate while still using plasma heating as the main mechanism for evaporation. The thruster anode, which also served as the propellant reservoir, was designed such that the open area was too low for sufficient vapor flow at normal operating temperatures (i.e. plasma heating alone). The remaining heat needed to achieve enough vapor flow to sustain thruster discharge came from a counter-wound resistive heater located behind the anode. The control system has the ability to arrest thermal runaway in a direct evaporation feed system and stabilize the discharge current during voltage-limited operation. A proportional-integral-derivative control algorithm was implemented to enable automated operation of the mass flow control system using the discharge current as the measured variable and the anode heater current as the controlled parameter. Steady-state operation at constant voltage with discharge current excursions less than 0.35 A was demonstrated for 70 min. Using this long-duration method, stable operation was achieved with heater powers as low as 6% of the total discharge power.

Using the thermal mass flow control system the thruster operated stably enough and long enough that performance measurements could be obtained and compared to the

performance of the thruster using xenon propellant. It was found that when operated with magnesium, the thruster has thrust ranging from 34 mN at 200 V to 39 mN at 300 V with 1.7 mg/s of propellant. It was found to have 27 mN of thrust at 300 V using 1.0 mg/s of propellant. The thrust-to-power ratio ranged from 24 mN/kW at 200 V to 18 mN/kW at 300 volts. The specific impulse was 2000 s at 200 V and upwards of 2700 s at 300 V. The anode efficiency was found to be ~23% using magnesium, which is substantially lower than the 40% anode efficiency of xenon at approximately equivalent molar flow rates.

Measurements in the plasma plume of the thruster—operated using magnesium and xenon propellants—were obtained using a Faraday probe to measure off-axis current distribution, a retarding potential analyzer to measure ion energy, and a double Langmuir probe to measure plasma density, electron temperature, and plasma potential. Additionally, the off axis current distributions and ion energy distributions were compared to measurements made in krypton and bismuth plasmas obtained in previous studies of the same thruster. Comparisons showed that magnesium had the largest beam divergence of the four propellants while the others had similar divergence. The comparisons also showed that magnesium and krypton both had very low voltage utilization compared to xenon and bismuth. It is likely that the differences in plume structure are due to the atomic differences between the propellants; the ionization mean free path goes down with increasing atomic mass. Magnesium and krypton have long ionization mean free paths and therefore require physically larger thruster dimensions for efficient thruster operation and would benefit from magnetic shielding.

Chapter 1

Introduction

1.1. Introduction and Motivation

Hall-effect thrusters (HETs) are a type of electric propulsion device that uses crossed electric and magnetic fields to ionize and accelerate gaseous propellants to very high exhaust velocities. Hall thrusters have very long lives and are well suited for use on communication satellites for station-keeping missions, for orbit raising, as well as for use on deep space probes. The most common Hall thruster propellant is xenon. It has a large atomic mass, 131 amu, enabling a large thrust-to-power ratio; it has a relatively low first ionization potential, allowing for efficient propellant ionization; and it is a gas when it is delivered to the thruster enabling the use of pressure gradients and well-known technology to control the mass flow rate. When operating on xenon propellant, Hall thrusters can achieve specific impulses between 1600 s and 3500 s with efficiencies greater than 50%.

Due to their relatively simple design, high ionization efficiency, and long life, Hall thrusters are ideal propulsion devices for many different types of space missions. For this reason, Hall thrusters have been very well characterized and have been the subject of extensive research. Hall thruster development in the United States took off in the 1990s with studies of the main physical processes, high frequency oscillations in the plasma

discharge, and the energy transport properties of the plasma [1-3]. Later research was aimed at increasing the operational envelope of Hall thrusters. Research performed by Hofer, Gallimore, and Jankovsky investigated the potential of increasing the range of attainable specific impulse by altering the magnetic field to allow for high-voltage operation without efficiency losses [4-6].

Condensable propellants, that is, propellants that are solid at ambient temperatures, offer benefits over xenon for certain Hall thruster missions. Condensable propellants expand the range of attainable specific impulse (Isp) and thrust-to-power ratio compared to what is possible with xenon. From a mission perspective, the expanded range of Isp and thrust-to-power can translate into mass savings, power savings, or both when compared to xenon. Furthermore, because condensable propellants are solid at room temperature, they condense on the room-temperature walls of vacuum test facilities after being expelled from the thruster, and for this reason are often referred to as "self-pumping"; this reduces the need for expensive pumping systems and greatly decreases the development cost associated with high-power thrusters. Bismuth, zinc, iodine, and magnesium are four of the most practical condensable propellants, though others have been explored by Soviet researchers [7]. Bismuth, for example, has a lower ionization potential than xenon and has the highest atomic mass of the non-radioactive elements allowing for a higher achievable thrust-to-power than xenon when operated at the same discharge voltage. Iodine is very similar in performance to xenon, but is much less expensive and has a higher storage density [8]. Zinc and magnesium have lower ionization potentials than xenon, and their lower masses allow for a higher specific impulse than xenon at the same discharge voltage. Magnesium is a particularly promising

Hall thruster propellant. It has a low atomic mass compared to xenon allowing for attainable specific impulses on the order of 4000 s at 300 V discharge. Missions using magnesium as a propellant have the possibility of in-situ refueling as magnesium is found in both Martian and lunar regolith [9,10].

Research into the use of condensable propellants in Hall thrusters began with Soviet researchers as early as the 1960s [7]. While many condensable propellants were tested, bismuth was studied extensively in the TsNIIMASH program as a propellant for a high power thruster with anode layer [11]. This work was then extended in the Very High Isp Thruster with Anode Layer (VHITAL) program in the United States in 2005 [12], in which bismuth was to be used as a propellant for a thruster with a specific impulse on the order of 6000-8000 s. At the same time, bismuth was examined by Massey, King, and Makela for use in a 2 kW Hall thruster [13-17], however the temperatures required for the sustained use of bismuth caused catastrophic material failures [15].

In 2009 researchers in the Ion Space Propulsion (ISP) lab at Michigan Technological University performed experiments using zinc and magnesium as Hall thruster propellants [18-20]. Magnesium and zinc were ideal propellants over bismuth due to their high vapor pressures at much lower temperatures than bismuth eliminating the material failures [20]. Other research into condensable propellants was performed by Busek Co. where bismuth, magnesium, zinc, and iodine have been investigated [8,21,22].

1.2. Goal of Research

While magnesium has been used as a Hall thruster propellant, stable operation has not been demonstrated in literature, nor have measurements of performance been published.

The goal of the research proposed in this document was to evaluate magnesium as a Hall thruster propellant. There were two important factors to consider: (1) thruster operation and performance using magnesium and (2) ground testing benefits. Performance and operation of the thruster were considered to be of the most importance and therefore dictated the evaluation of magnesium as a propellant. Prior to performance measurements, it was necessary to develop a method of thruster operation that would enable long-duration, stable operation of the thruster. Performance was evaluated by comparing measurements of thrust, specific impulse, thrust-to-power ratio, and efficiency using magnesium compared to xenon propellant at analogous operating conditions. Properties of the magnesium plasma beam were evaluated by making measurements of plasma potential, electron temperature, electron density, ion energy, and off-axis current distribution and comparing those measurements with measurements made using the same Hall thruster model operated using krypton, xenon, and bismuth propellants taken in other studies. Ground testing benefits were still evaluated—results in Appendix A—by measuring the background pressure of magnesium during operation but not considered definitive enough to include in evaluation of magnesium as a propellant.

As a direct result of this research, an efficient method of magnesium thruster operation was designed, implemented, and published. The performance of a xenon Hall thruster operated using magnesium propellant was also measured. Characteristics of the magnesium plasma beam were compared to measurements made in the plasma beams of krypton, xenon, and bismuth fueled thrusters of the same model. From the plasma measurements, changes to the thruster design are suggested to increase performance and efficiency of the thruster using magnesium and other propellants.

1.3. Structure of Document

The remainder of the document is broken up in the following way. Chapter 2 discloses the proper information and context to understand the benefits and reasons for using magnesium as a Hall thruster propellant as well as the difficulties and general concerns. First, the desirable qualities of magnesium as a propellant are examined through analysis of the rocket equation and other mission criteria. Then, the basic operation of Hall thrusters is examined and the important physical properties are discussed. Finally, the history of condensable propellant thrusters is addressed; in particular, a detailed discussion of thruster operation and propellant mass flow control is presented.

Following the discussion of mass flow control in condensable propellant thrusters and the associated difficulties, Chapter 3 presents an efficient method of mass flow control and thruster operation using magnesium propellant. The origin of the method is explained followed by the experiments demonstrating the technique. Using the mass flow control technique laid out in Chapter 3, the performance of the thruster is characterized in Chapter 4 and compared to xenon using all of the same thruster hardware including the supplemental heater. Chapter 5 then examines the plasma structure of the magnesium-fueled thruster and compares it to that of krypton, xenon, and bismuth, ending with suggestions for design considerations when choosing a light propellant such as magnesium.

A summary of the work performed and the corresponding implications is presented in Chapter 6 along with suggestions for future work and experiments. Two appendices

follow describing a technique for measuring the background pressure of magnesium during thruster operation as well as the modification of a 5 kW thruster for operation on magnesium using a scaled design of the mass flow control system presented in Chapter 3.

Chapter 2

Background

2.1. Why Magnesium Propellant?

The first question to be addressed by this dissertation is: "Why magnesium propellant?" To answer this question first we must address the province of Hall thrusters and electric propulsion in general and where magnesium fits in to the paradigm. The best way to put electric propulsion into perspective is to examine the rocket equation:

$$m_f = m_i e^{\Delta v / g I_{sp}} \tag{1}$$

where m_f is the final mass of the spacecraft, m_i is the initial mass of the spacecraft including all necessary propellant, Δv is the total change in velocity needed for the mission (delta-V), and I_{sp} is the specific impulse of the spacecraft related to the exhaust velocity, v_e, of the thruster propellant by $v_e = gI_{sp}$. From equation (1) it can be seen that in order to have a large mass fraction for the delivered payload the specific impulse of the thruster must be on the order of the total delta-V. Electric propulsion devices are characterized by very large specific impulse thrusters—greater than 1000 s. Commercial

Hall thrusters using xenon propellant generally achieve specific impulses on the order of 1600 s with a 300 V acceleration potential.

From equation (1) it would seem that a high specific impulse is always desirable. Unfortunately there is a compromise that comes with increased specific impulse. In the case of an electric rocket thrust, T, and specific impulse, I_{sp}, are related by $TI_{sp} = 2\eta P/g$ where η is thruster efficiency and P is discharge power. During a mission power is inherently limited to some finite value, so there is a tradeoff between thrust and specific impulse. An increase in specific impulse increases the mass efficiency (i.e. increased delivered mass) while also decreasing the thrust thereby increasing trip time.

In order to enable different missions, thrusters need to be operable over a range of specific impulses. There are two ways to change specific impulse as seen in equation (2): through changes in acceleration potential, V, or molecular mass, M.

$$I_{sp} \propto \sqrt{\frac{V}{M}} \tag{2}$$

Significant work has been performed to enable efficient operation of thrusters at high discharge voltage [4-6] such that an I_{sp} upwards of 3000 s can be achieved. The second method of changing specific impulse is to change the propellant mass. The atomic mass of xenon is 131 AMU compared to 24 AMU for magnesium for a specific impulse increase of ~2.2.

Because of the innately high specific impulse of magnesium-fueled thrusters, they would lend themselves well for deep-space and/or Discovery class missions. One mission architecture well-suited for a magnesium Hall thruster would be so-called small body missions as analyzed by Dankanich [23]. In his analysis Dankanich looked at several

thruster options for a Dawn-like mission to several asteroid targets using solar electric propulsion (SEP). For his notional mission, Dankanich compared the NEXT ion thruster, HiVHAC Hall thruster and the XR-5 (BPT-4000). Dankanich concluded that the NEXT ion thruster would be the system of choice due to the reduction in propellant needed to complete the mission due to the higher achievable specific impulse of the NEXT ion thruster compared to the two Hall thruster systems. However, it has been shown that Hall thruster systems have significant cost advantages to ion thruster systems [24,25]—greater than $6M. The NEXT ion thruster is rated as having a specific impulse of ~4200 s [26] which would be easily matched by a magnesium HET at ~300 V. In addition to the cost savings of switching to an HET from and ion thruster, a magnesium thruster would save an additional $1M on propellant: 500 kg of xenon at ~$1700/kg as compared to ~$200/kg for magnesium. All of these savings are important for a cost-capped Discovery mission.

Other high impulse interplanetary missions may also be enhanced by the use of magnesium-fueled Hall thrusters. The Human Exploration Framework Team (HEFT) has identified solar electric propulsion as an enabling technology for future missions, citing the mass savings due to the achievable specific impulse [27,28]. Magnesium Hall thrusters could be of major benefit these missions in two ways: (1) magnesium thrusters could achieve relatively high specific impulse at low voltages—2000 s at 100 V—and (2) magnesium is available in high quantity on the surface of Mars [10].

The first benefit—high Isp at low voltage—is a mass savings benefit. Hoffman et al. [29] identified high power Hall thrusters (eight 38 kW HETs or ten 30 kW HETs) operating at 2000 s to be a reasonable choice to balance trip time and mass efficiency for the HEFT design reference mission (DRM) to a near-Earth asteroid. Additionally, it was

shown that eliminating the voltage conversion from the power processing unit (PPU) could reduce the unit mass by more than 50%. A block diagram of an electric propulsion satellite power system is shown in Fig. 1.

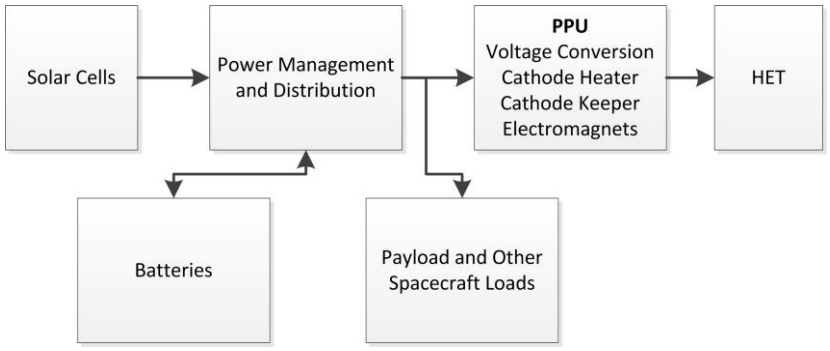

Fig. 1. Power distribution from solar cells to the Hall thruster. Elimination of the voltage conversion for Hall thruster operation would eliminate significant mass.

Since the mission is looking at a total propulsive power of ~300 kW the PPU would account for ~500 kg (assuming PPU specific mass of 1.7 kg/kW [30]). Reducing the mass by 250 kg would be significant, but removing the voltage conversion stage of the PPU would reduce the available voltage for thruster operation to that of the bus voltage of the solar panels—approximately 80-160 V. It has been posited that direct drive architectures could be made to operate at 300 V but significant improvements to solar array technology would be required [31]. A xenon HET operating at 80-160 V, bus voltage, would only be able to achieve a specific impulse of less than 1500 s [32] while a magnesium thruster at 100 V could theoretically achieve a specific impulse of 2000 s maintaining the mission requirement with significantly lower mass.

The second benefit of Magnesium thrusters for HEFT missions—the availability of magnesium on the surface of Mars—relates to another major goal of HEFT which is in-situ resource use (ISRU). Magnesium is available in its oxide state on the surface of Mars

in quantities of at least 3% of soil composition as determined by the Viking landers [28]. Refinement of the magnesium on the surface could be used for refueling magnesium Hall thrusters for cargo missions as well as refueling magnesium solid rockets. Moreover, if the technology was provided to refine magnesium from the soil, then it could also be used in creating lightweight structural materials as is done terrestrially. While magnesium is not the easiest resource to extract from its oxide states, there would be multiple benefits to developing the capability. Currently there are active research efforts aimed at producing magnesium on Earth [33] in efficient, clean ways. These research efforts could also be directed towards developing a refinement method suitable for use in a Mars mission.

A general benefit of magnesium thrusters is the elimination of the need for a pressure vessel for propellant storage. Xenon-fueled HETs require that xenon be stored at high-pressure and density. Supercritical xenon can be stored at 1.6 g/cm^3 in a pressure vessel. Magnesium has a density of 1.7 g/cm^3 in its solid form and does not require a pressure vessel [22]. Using the model from Hofer and Randolph the mass of the tank + propellant for a xenon fuel system can be scaled from the Dawn mission where a 19 kg tank was required for 425 kg of xenon [30]. It has been estimated that a large SEP vehicle could require 30,000 kg of xenon such that a 1300 kg pressure vessel may be required [31]. In this case magnesium would save mass and cost. Capadona et al. [31] pointed out that the 30000 kg of xenon required for a high-power SEP mission could consume in excess of 50% of the yearly global production of xenon which could have drastic consequences on the price of the propellant. Even if the xenon price remained stagnant at $1700/kg the cost would be $51M for xenon compared to $6M for magnesium. Also the production of

magnesium in the U.S. was greater than 63,500,000 kg in 2011 [34] such that the market could would likely be able to absorb the extra demand.

Another area in which magnesium thrusters may provide major benefits is in the area of small satellite propulsion. Many small satellites are secondary payloads and have restrictions on stored energy: i.e. reactive propellant and pressure vessels. Therefore direct-drive magnesium Hall thrusters may enable low mass propulsion systems without the need for a pressure vessel. Magnesium also has the benefit of being stored for long periods of time without degradation. Successful operation of magnesium Hall thrusters was performed with 20-year-old magnesium turnings purchased in the mid-1990s.

According to the 2012 NASA In-Space Propulsion System Roadmap, future missions for Hall thrusters will require 10s to 100s of kW [35]. These high power thrusters will only be operable in a handful of government facilities, and even fewer, if any, university scale facilities. This is due to the very high propellant throughput in a high-power thruster. Very high capacity cryogenic vacuum pumps are necessary to maintain suitable background pressures to simulate on-orbit operation. One such facility capable of testing high power thrusters is NASA Glenn's VF-5 facility boasts a pumping speed greater than 5 million liters per second of xenon. Only academic facilities at Georgia Tech, and the University of Michigan have space simulation chambers which approach the necessary pumping capacity with pumping speeds of ~200,000 liters per second of xenon. However according to Dankanich et al. [36] for a 50 kW thruster the facility needs a xenon pumping speed of ~400,000 liters per second to reliably measure performance, ~1,400,000 liters per second to reliably measure near-field plasma properties, and more than 3,000,000 liters per second to obtain lifetime data. Even the facilities at Georgia

Tech and The University of Michigan do not have sufficient capability for testing other than performance for most high power thrusters. With limited resources for ground testing, parallel development of high-power thrusters will be stifled, slowing technology development.

A solution to the development of high power thrusters is presented using condensable propellants like magnesium. Beyond the performance benefits, magnesium also has major developmental benefits for the ground testing of Hall thrusters. First, like all other condensable propellants, magnesium has a very low vapor pressure at room temperature such that it condenses from the gas phase to the solid phase on any room temperature surface after being expelled from the thruster. This is very attractive as it could enable high fidelity performance measurements of high power thrusters using university-scale vacuum facilities without using high-capacity cryogenic pumping systems. Moreover, once condensed on the walls of the vacuum facility, magnesium may act as a getter material and further reduce the pressure inside the facility [37,38]. This could enable high-fidelity measurements in facilities with only modest pumping speeds. While the condensable nature of magnesium is a major benefit during ground testing, it is a major detriment while on-orbit. Backflowing propellant that exists at all off-axis angles around a thruster [3] can, in the case of magnesium and as well as other condensable propellants, not only sputter spacecraft surfaces but may also condense on them. The conductive optically opaque surface may be a detriment to optical surfaces, solar panels, and electronics. However, the judicious use of beam shields to block the propellant backflow could mitigate the issue.

One final, one might even call “exotic”, benefit of magnesium would be the recycling of spacecraft structures as propellant. Because magnesium can form a sturdy light-weight spacecraft structure, one could envision architectures where portions of the structure are constructed of magnesium which could be absorbed into the propulsion system as the components are no longer needed. This is a unique capability of magnesium propellant and could prove beneficial for certain missions.

2.2. Hall Thrusters

Hall-effect thrusters are a type of ExB plasma device used for spacecraft propulsion. Hall thrusters are cylindrical devices with axial symmetry in the plasma discharge. An axial electric field crossed with a predominately radial magnetic field is used to confine electrons in an azimuthal drift; gaseous propellant is fed through the confined electrons and is ionized through electron-impact ionization [2,4,39]. The ions are then expelled from the device via the axial magnetic field at very high velocities ranging from 10,000 m/s to greater than 30,000 m/s depending on the device [4]. For Hall thrusters to operate properly, the thruster dimensions must be such that the Larmor radius of the electrons is small compared to the thruster diameter, while the Larmor radius of the ions must be much larger than the thruster diameter—i.e. the electrons should be magnetized and the ions should not be magnetized. A schematic highlighting the major physics of a Hall thruster is shown in Fig. 2.

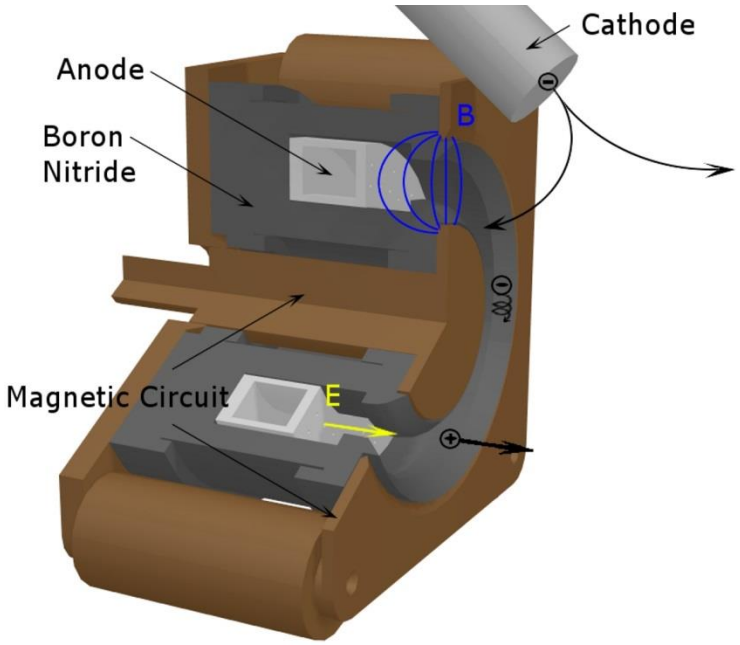

Fig. 2. Quarter section of a Hall-effect thruster highlighting all of the major components and fields.

It is the physics internal to the thruster that determine the performance of the thruster and the overall shape and composition of the plasma beam. The main features determining the properties of the plasma beam are the so-called ionization and acceleration regions—the locations of which tend to overlap. Electrons traveling toward the anode are impeded by the magnetic field and form equipotentials that follow the field lines [40]. Ideally the propellant is ionized upstream of the ionization/acceleration region where the local plasma potential is high and then are accelerated quickly through a region of high axial electric field gradient [2]. If an atom is ionized later in the acceleration region, then the energy it accrues will be lower due to the lower plasma potentials encountered further downstream. In addition to ionization and overall ion energy, it has also been shown that the potential structure of the acceleration region is related to the plume divergence [41-43]. Generally the magnetic field of modern Hall thrusters is

shaped such that the field lines are concave with respect to the channel centerline—aptly named the magnetic lens configuration. Because the electrons tend to form equipotential lines nearly parallel with the magnetic field lines, a focusing effect is observed [41-43]. Because different atomic species have different ionization characteristics, their interaction with the ionization and acceleration regions are going to be different. This is an important interaction when studying a new propellant.

In order to quantitatively analyze thruster performance a number of researchers have collectively developed an efficiency architecture which breaks down the total thruster efficiency into a number of separate components [2,4,32]. While a detailed overview of the efficiency architecture is beyond the scope of this document, the following overview of the relevant parameters provides a method of evaluating thruster loss mechanisms in Chapter 5. The most ubiquitous measurement of efficiency is the so-called thrust efficiency, η_T given by

$$\eta_T = \frac{T^2}{2\dot{m}P_d} \tag{3}$$

where T is thrust as measured by thrust stand, $\dot{m}$ is the mass flow rate of propellant, and P_d is the discharge power (discharge voltage multiplied by discharge current). Essentially the thrust efficiency is a measure how well the thruster converts electrical power and mass into propulsive thrust.

Additional efficiency metrics are rigorously derived by Brown [32] including beam efficiency, η_B, and voltage utilization efficiency, η_V, a sub-parameter of the energy efficiency. Beam efficiency is the ratio of the axially directed beam current, I_{axial}, and the

total beam current, I_{beam}, as shown in equation (4) where $i(\theta)$ is the current density swept over an arc at a radius, R, from the thruster face. A schematic of the analysis is shown in Fig. 3. The beam efficiency tends towards unity in the case that the beam is directed axially away from the thruster with minimum cosine losses.

$$\eta_B = \left(\frac{I_{axial}}{I_{beam}} \right)^2 = \left(\frac{2\pi R^2 \int_{-90°}^{0°} i(\theta)\cos(\theta)\sin(\theta)d\theta}{2\pi R^2 \int_{-90°}^{0°} i(\theta)\sin(\theta)d\theta} \right)^2 \quad (4)$$

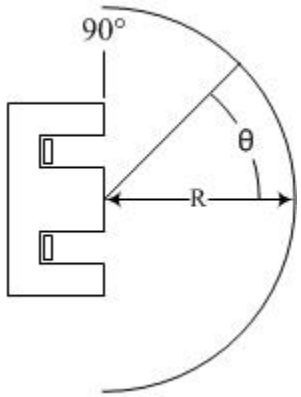

Fig. 3. A schematic highlighting the components of equation (4).

Voltage utilization is a measure of how well the thruster ionizes and accelerates propellants. Ideally the propellant is singly ionized upstream of the acceleration region and accelerated fully utilizing the discharge voltage. Variations in ion energy represent inefficiency. The voltage utilization efficiency is determined using equation (5), where V_{mp} is the most probable ion voltage as measured by a retarding potential analyzer (RPA), V_p is the plasma potential measured by a Langmuir probe at the location of the RPA, and V_d is the discharge voltage.

$$\eta_V = \frac{V_{mp} - V_p}{V_d} \tag{5}$$

2.3. Facility Effects

When developing a thruster it is important to be able to predict on-orbit performance. The main method for predicting on-orbit performance is to test the rocket in ground facilities that simulate the space environment. To this end Hall thrusters are tested in large vacuum facilities equipped with large high-capacity vacuum pumps—generally cryogenic pumps. Using high-capacity vacuum pumps, large facilities can reach base pressures on the order of 10^{-7} torr; the goal of testing in these large high-vacuum facilities is to match the volume and vacuum into which the thruster plume may expand in space. Any differences in the ground-testing environment and the in-space environment may translate into performance discrepancies during in-space operation. Many studies have been performed to document the discrepancies between the performance of a thruster during a ground test and the in-space performance—referred to as facility effects. Starting as early as the 1990s, standards were proposed [44,45] due to the noticeable effects that facility pressure and size had on performance of a thruster.

During performance tests, the thrust, specific impulse, and efficiency of a Hall thruster are measured. Each of these measurements is dependent on the mass flow rate of the thruster. Therefore it is important to know the mass flow rate of the thruster precisely. However the background gas can effectively increase the mass flow rate due to random diffusion into the discharge chamber of the thruster. This re-circulation of background gas can then be ionized and expelled from the thruster artificially modifying operation

parameters. Using kinetic theory, the thermal effusion of the background gas into the discharge chamber can be calculated using the following equation:

$$\phi = \frac{1}{4} n \sqrt{\frac{8 k_B T}{\pi M}} = \frac{P}{\sqrt{2 \pi M k_B T}} \tag{6}$$

In equation (6) ϕ is the particle flux, n is the number density, T is the temperature, M is the molecular mass, and P is the background gas pressure. The added mass flow rate from the background gas is then

$$\dot{m} = \phi M A \tag{7}$$

where A is the area through which background gas can enter the discharge chamber. It has been shown, however, that the amount of ingested gas needed to explain the discrepancies between thruster performance at low pressures and thruster performance at higher pressures is well above the ingested flow rate predicted by kinetic theory [46,47].

In addition to modifying the performance of a thruster, the ground test facility can also affect the expansion of the plasma beam, which has implications in the area of plasma diagnostics in the thruster beam and the prediction of thruster-spacecraft interaction. It was found by Walker that there is a large increase in ions at high off axis angles in the plasma beam due to increased charge exchange collisions [48]. Though, probes have been created that work to correct the inflated measurement of off-axis ions [49].

While some facility effects can be corrected using specialized probes or mathematical corrections, the best way to predict in-space performance is still to simulate the in-space environment in better ways—i.e. higher vacuum and larger vacuum facilities. However, the current trend in Hall thruster design is towards higher and higher powers approaching

hundreds of kilowatts, such that even the best facilities can only operate these thrusters at 10^{-5} torr. One of the major benefits of condensable propellants may be that high power testing can be done without the need for high-capacity cryogenic pumps because the spent propellant condenses on any room temperature surface in the vacuum facility.

2.4. Condensable Propellant Hall Thrusters

The biggest difference between condensable propellants and gaseous propellants is the mass flow control system. Gaseous propellants are stored in pressure vessels and delivered to the thruster via plumbing and metered flow controllers. Condensable propellants are solid at ambient temperatures and must therefore be vaporized before being delivered to the thruster discharge chamber. The evaporative mass flow rate, $\dot{m}$, of a condensable propellant can be predicted using the following equation:

$$\dot{m} = \frac{P_v(T_p)}{\sqrt{\frac{2\pi k_B T_p}{M}}} A_{open} \tag{8}$$

where $P_v(T_p)$ is the temperature-dependent vapor pressure of the propellant, T_p is the temperature of the propellant, M is the atomic mass of the propellant species, and A_{open} is the open area (the area through which the vapor can flow). Thus to specify and control a mass flow rate in an evaporative system one must have control of either the free surface area or the free surface temperature.

Past experiments using condensable propellant Hall thrusters employed several different mass flow control systems. High-power bismuth Hall thrusters developed by TsNIIMASH in the 1960s–1980s used a resistively heated propellant reservoir that was

mechanically separated from the thruster head, delivering hot vapors to the thruster via heated propellant lines [11]. This propellant feed system was sufficient to allow for thruster operation but was not practical for a flight application. In 2005 NASA researchers re-evaluated the TsNIIMASH thruster in the Very High Isp Thruster with Anode Layer (VHITAL) program [12]. As part of the program, a feed system was developed that used an electromagnetic pump to feed liquid bismuth into a porous carbon vaporizer [50]. The feed system was demonstrated by Polzin et al and was able to provide up to 6 mg/s of bismuth vapor, but the mass flow control system was never integrated with a Hall thruster.

In 2009 researchers at Busek Co. developed another mass flow control system for condensable propellant thrusters. By employing long wires of zinc and magnesium, Szabo et al [21] were able to demonstrate a wire propellant feed/mass flow control system. Zinc and magnesium wires were fed into a heated vaporizer tube. This system was able to produce zinc flow rates of greater than 1 mg/s at ~40 W heater power, and magnesium flow rates of 0.8 mg/s at 80 W heater power [21]. Later work by Szabo demonstrated thruster operation using a more mature version of the magnesium wire feed system [22].

Massey and King studied another alternative flow control system that did not rely on a mechanically separate evaporator. In 2004 Massey et al [16] began work developing a 2-kW bismuth-fueled thruster that would be self-sustaining during operation; no additional power would be needed to vaporize propellant. In his experiments Massey developed an anode that acted as the propellant reservoir, gas distributor, and ion accelerator [15,17,51]. The anode was hollow with a porous face, such that liquid

bismuth would reside in the anode while allowing the vapors to escape through the porous face. The heat required for propellant vaporization was supplied directly from the thruster discharge due to Joule heating at the anode face from the plasma current, and so the method was aptly named the "direct-evaporation method." The direct-evaporation method offers a unique benefit over the other mass flow control systems that have been studied in the past: there is no system efficiency penalty from external heating. The power needed to heat and evaporate propellant is provided by waste heat from the thruster discharge. A depiction of the direct-evaporation method is shown schematically in Fig. 4. Unfortunately, the temperatures needed for suitable bismuth evaporation strained the material limits of the thruster and the method proved unreliable for use with bismuth [15]. Magnesium and zinc, which require much lower temperatures than bismuth to produce necessary vapor flow, proved to be better propellants for the direct-evaporation method [20]. Experiments performed by Makela et al demonstrated the world's first Hall thruster operating on zinc, and the first operation of a Hall thruster on magnesium since the end of Soviet research on condensable thrusters. Magnesium demonstrated the most attractive operation as its low vapor pressure and high melting point enabled sublimation of propellant rather than evaporation, such that all propellant handling occurred in the solid state.

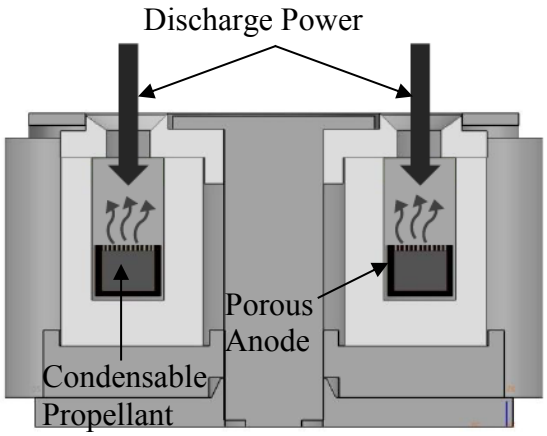

Fig. 4. Cross-section of Hall thruster illustrating the direct-evaporation method. Heat from the plasma discharge evaporates the propellant stored inside the anode. Vapors escape through the porous face of the anode into the discharge chamber.

In order to control the operating conditions such as thrust and specific impulse in a Hall thruster, it is necessary to drive the discharge with power supplies in constant-voltage mode, such that the exit velocity of the propellant and therefore the specific impulse of the thruster are selected through the discharge voltage. Unfortunately, constant-voltage operation is inherently problematic for thrusters using the direct-evaporation method. Because the open area of the anode is fixed, the mass flow rate of a thruster employing the direct-evaporation method depends only on Joule heating caused by the discharge current attached to the anode. If there is a perturbation in the discharge current and the discharge power decreases, then the temperature of the anode and propellant will decrease causing a decrease in the propellant evaporation rate. The decrease in propellant flow will cause a corresponding decrease in discharge current and discharge power, resulting in a further decrease in the propellant flow rate. If there is a perturbation and the discharge power increases, then the temperature of the anode and propellant will increase, causing an increase in the propellant flow rate. The increase in

propellant flow will cause a corresponding increase in discharge current and therefore discharge power, resulting in further increase in the propellant flow rate. These thermal runaway instabilities are referred to as “cold runaway” and “hot runaway” respectively. It is important to note that there is no stable operating point for a direct-evaporation thruster in constant-voltage mode; the thruster is always either in hot runaway or cold runaway.

In an attempt to actively control thermal runaway in a direct-evaporation condensable propellant Hall thruster, a series of experiments were performed by Kieckhafer et al to demonstrate thermal control of a Hall thruster anode using shim electrodes [52]. Ordinarily a Hall thruster is operated with a single anode; in Kieckhafer’s experiments an additional set of electrodes were placed downstream of the main anode as shown in Fig. 5. By increasing and decreasing the potential of the shims with respect to the main anode, the discharge current could be shared between the two sets of electrodes. Increasing the potential of the shims and removing current from the main anode decreased the Joule heating, lowering the temperature of the anode. By lowering the temperature of the main anode a hot runaway condition could be arrested in a direct evaporation thruster. Decreasing the potential of the shims and increasing the current attached to the main anode increased the Joule heating, increasing the temperature of the main anode. Adding current to the main anode from the shims could arrest a cold runaway condition. Kieckhafer’s experiments were successful in demonstrating the ability to raise and lower the anode temperature of a xenon hall thruster with a control window of 50° C [52]. Later, experiments performed by Massey used shims to provide thermal control of a direct-evaporation bismuth Hall thruster [15]. Unfortunately, the addition of shims to Massey’s thruster had unintended consequences: (1) the thruster would not operate

properly with the shims and (2) the inner shim became inexplicably hot even when electrically floating. Upon removing the shims Massey's thruster operated properly, but the thruster was always in a slowly growing runaway mode that could not easily be arrested [15]. The ability of shim anodes to provide governance of mass flow rate in a direct evaporation magnesium thruster was demonstrated by Makela [20] and Hopkins [19], but only at low voltages (<160 V) and only for periods of a few minutes.

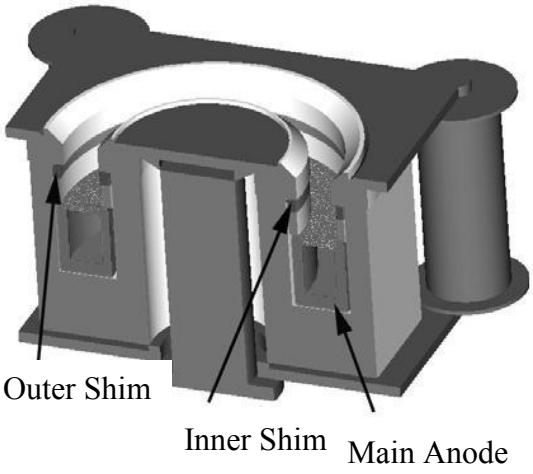

Fig. 5. A sectional view of a modified BPT-2000 Hall thruster showing the location of the shim electrodes used in Kieckhafer's experiments.

Because of the problems with shim anodes, Massey and Makela devised an alternative temperature control scheme in which they operated their thrusters using power supplies in constant-current mode without shims [15,17,20,51]. By operating a direct-evaporation thruster in constant-current mode, the discharge power supply served to passively stabilize the propellant mass flow rate. In constant-current mode, if there is a perturbation and discharge power (and thus anode temperature) increases, then the mass flow rate increases. Due to the I-V characteristics of a Hall-effect discharge, an increase in mass flow rate—with current held constant—will cause a decrease in the discharge

voltage and a decrease in the discharge power, arresting the runaway. If the converse happens and discharge power decreases, then the mass flow rate will decrease, causing an increase in the discharge voltage. The increase in discharge voltage will increase the discharge power, arresting the runaway mass flow rate. While constant-current operation of the direct-evaporation magnesium thruster enabled stability at a prescribed current set-point, the discharge voltage was uncontrolled and naturally stabilized around 130 V for the particular thruster used in the tests. Attempts were made to vary the naturally stable voltage through mechanical design [19], but the constant-current approach was deemed impractical since the voltage, and hence Isp, could not be specified.

Chapter 3

Thermal Mass Flow Control[1]

In order for direct-evaporation condensable propellant thrusters to be a viable technology they must be able to operate stably in constant-voltage mode with a discharge voltage that can be directly specified and changed over a mission-relevant range. Previous studies have focused on two methodologies for controlling the mass flow rate of condensable propellants: (1) externally located propellant reservoirs connected to the thruster head via heated propellant lines where external heat sources control the propellant evaporation rate [7,11,12,21,22,50,53,54] and (2) internally located propellant reservoirs where the anode holds the propellant and the waste heat from the plasma discharge controls the propellant evaporation rate [15,18-20,55]. Both methods have major benefits and major detractions: method (1) offers precise control over the mass flow rate but suffers major inefficiencies due to additional heater power and method (2) needs no additional heating for propellant evaporation but because the mass flow rate is coupled to the discharge conditions, the mass flow rate is unstable. The work presented in this chapter describes a method for condensable propellant mass flow control, which needs very little additional heat while maintaining precise control of the mass flow rate.

[1] The majority of this chapter appears in the publication: "Magnesium Hall Thruster with Active Thermal Mass Flow Control," Journal of Propulsion and Power, 30, 2014, pp. 637-644, by Mark A Hopkins and Lyon B. King. Copyright retained by Mark A. Hopkins.

3.1. Goal of Experiment

While the shim anode approach was unsuccessful for use in direct evaporation Hall thrusters, the experiments associated with development of this technique have demonstrated two important points: (1) the natural plasma discharge heat input to a Hall thruster anode is of sufficient magnitude to evaporate condensable propellants at rates commensurate with normal operation, and (2) the evaporation rate from the anode can be adjusted by adding or subtracting small amounts of heat to/from the evaporative anode [15,52]. The goal of the work reported in this chapter is to capture the primary benefit of the direct-evaporation scheme, namely to use plasma discharge waste heat to drive the evaporation, but to abandon the shim-anode control technique in favor of a straightforward supplemental resistive heater used to augment the plasma heating. In this manner the mass-flow control is largely uncoupled from the thruster plasma discharge conditions yet system efficiency is preserved.

3.2. Experimental Setup and Description of Apparatus

The mass flow control system used in the experiments presented here utilized the waste heat of the thruster discharge to evaporate the propellant, as done in the direct evaporation method, but also included a supplemental resistive heater located behind the anode to provide fine temperature control. The most critical component of this design was the anode. The anode needed to be hollow and able to store enough propellant for each test. Also, the anode open area, that is, the area through which vapors can flow through the porous face, needed to be chosen carefully. If the open area was too great

then the ambient anode temperature during operation would cause excessive mass flow and constant voltage mode would be impossible (e.g. not possible to actively cool the anode). If the open area was too small then an excessive amount of supplemental heater power would be required to sufficiently increase the anode temperature over its ambient value to achieve the desired evaporation. Based on previous experiments [18,19], a hollow anode with open area 14.8 x 10^{-6} m^2 was fabricated.

The thruster described here was a modified Aerojet BPT-2000 Hall-effect thruster [56]. The magnetic circuit design of the original thruster has been preserved, but the boron nitride body has been modified to allow the addition of a resistive tungsten heater behind the anode. A cross-section of the thruster highlighting the location of the anode heater is shown Fig. 6. The modifications to the boron nitride body to house the anode heater are shown in Fig. 7. Because several amps of current must be applied to the anode heater, the tungsten wire is wrapped with alternating coils to ensure that the heater does not induce an axial magnetic field.

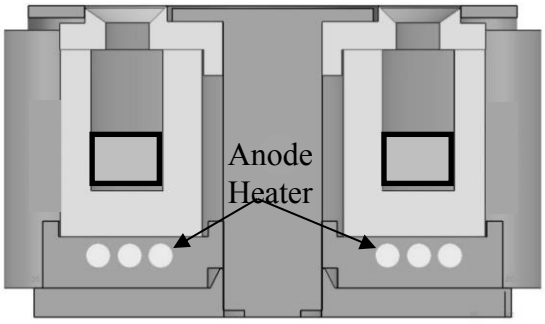

Fig. 6. A cross-sectional view of the BPT-2000 Hall thruster is shown, highlighting the location of the anode heater.

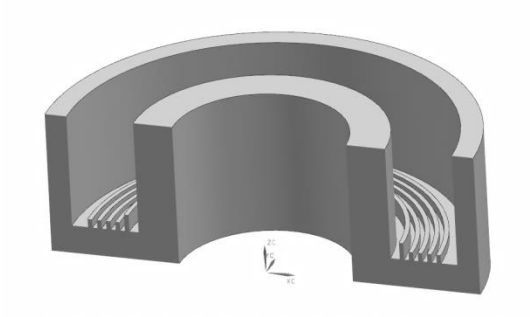

Fig. 7. The boron nitride body with groves machined to allow for the addition of a tungsten heater behind the anode.

All experiments were performed using a laboratory LaB_6 hollow cathode operated using a 10-sccm flow of argon gas. The thrust stand used in the experiments was a NASA-Glenn style, inverted-pendulum, null-displacement thrust stand. The vacuum facility used was a 2-m-diameter by 4-m-long vacuum facility with a pumping speed of 6000 liters-per-second provided by three turbomolecular pumps [51].

For each of the experiments reported in the following sections the same testing procedure was followed. First the anode was preloaded with propellant and the thruster was assembled. The thruster was then mounted in the vacuum facility. Once at vacuum the argon hollow cathode was ignited with discharge sustained on the cathode keeper electrode and the thruster was pre-heated by passing 400-450 W to the supplemental anode heater. The anode potential was set to 300 V when the heater was powered. After ~30 minutes the thruster ignited – usually in a current-limited mode with discharge voltage less than 300 V. The magnet current was then increased until the thruster switched to voltage-limited operation. The supplemental heater power was then reduced via techniques described below. During thruster operation, most, but not all, of the heat needed to vaporize the magnesium stored in the anode was provided by joule heating

from the plasma discharge, i.e. the direct evaporation method; additional heat was provided by the anode heater as needed to control the mass flow rate of the thruster.

3.3. Feasibility Test

As described in section III the most critical component in the mass flow control system presented here is the open area of the anode. The open area of the anode dictates the temperature range at which sufficient propellant vapors can flow through the porous face. The supplemental anode heater easily arrests cold runaway since the heater power can always be increased to further heat the anode and deliver a corresponding increase in mass flow. In order to arrest hot runaway it is crucial that the anode is designed with an open area too small to provide adequate mass flow to the thruster when heated by the plasma discharge alone: some amount of supplemental heater power must be required for stable operation. In this fashion the supplemental heater can provide control authority to arrest hot runaway by decreasing the heater power.

The first experiments performed were to demonstrate the feasibility of using the anode heater to arrest both hot and cold runaway. For each of the experiments the discharge voltage was at a constant 300 V and the current on the electromagnets was set at a constant 2.3 A. Three experiments were performed to evaluate the ability of the anode heater to control the mass flow rate of the thruster. Experiment 1 demonstrated the ability of the anode heater to arrest hot runaway by lowering the power to the anode and reducing its temperature. Experiment 2 demonstrated the ability of the anode heater to arrest cold runaway by increasing the power to the anode and increasing its temperature.

Experiment 3 demonstrates a manual bang-bang control system that demonstrates the ability to actively control mass flow by continually reversing the runaway conditions.

For Experiment 1, the thruster was already operating in voltage-limited mode at 300 V and a constant electromagnet current of 2.3 A. Initially the discharge current was increasing—and along with it the total power to the anode—indicating that the total heat input to the anode was too high and the thruster was in a hot runaway mode. In an attempt to arrest the increasing discharge current and mass flow rate, the heater power was manually reduced from 450 W to 280 W at 0.5 minutes and then further reduced to 100 W at 2.5 minutes. At 2.5 minutes the discharge current reached a maximum of 6.8 A and began to decline, showing that hot runaway was arrested. The results of this experiment can be seen in Fig. 8.

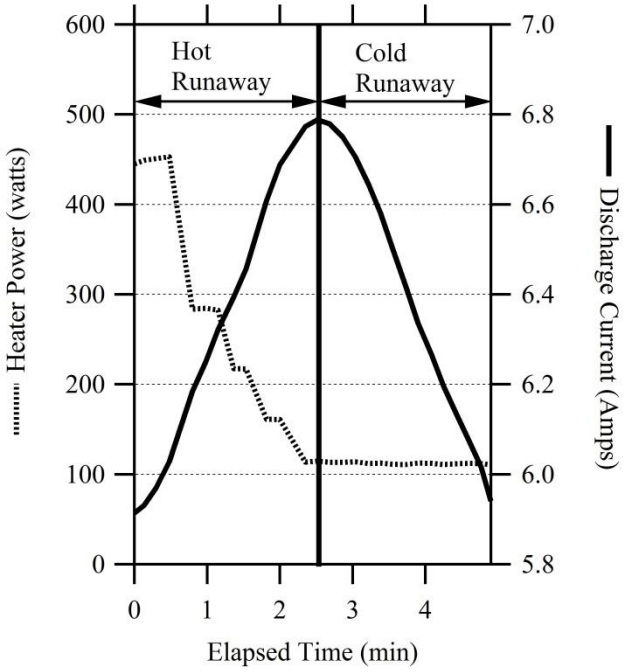

Fig. 8. A graph demonstrating the ability of the supplemental heater to arrest a hot runaway instability. Anode heater power is reduced at 0.5 minutes, cooling the anode and propellant. As the anode cools the

discharge current eventually reaches a maximum of 6.8 A at 2.5 minutes, and begins to decline. The discharge voltage was a constant 300 V and the current on the electromagnets was a constant 2.3 A.

For Experiment 2, the discharge current and mass flow rate were initially decreasing, indicating that the thruster was in cold runaway. At 0.5 minutes the heater power was manually increased from 100 W to 450 W. The discharge current reached a minimum of 5.85 A at 0.8 minutes and began to increase indicating an increase in the mass flow rate. The results of Experiment 2 where cold runaway was successfully arrested are shown in Fig. 9.

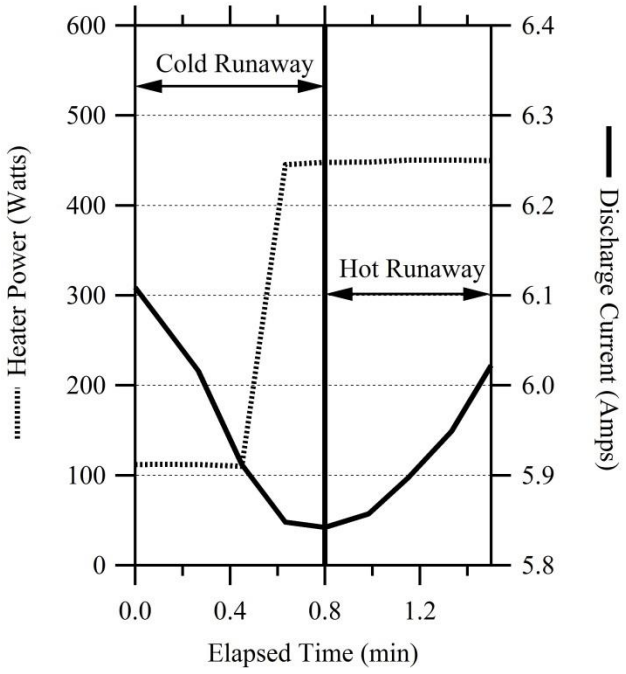

Fig. 9. A graph demonstrating the ability of the anode heater to arrest a cold runaway condition. At 0 min the discharge current is decreasing, signaling a decreasing mass flow rate. At 0.5 minutes the anode heater power is manually increased to 450 W. After the power to the anode heater increased the anode and propellant began heating as signified by the increasing discharge current and mass flow rate. The discharge voltage was constant at 300 V and the current to the electromagnets was a constant 2.3 A.

Experiment 1 and Experiment 2 demonstrated that the supplemental anode heater could be successfully used to prevent instability growth. Experiment 3 was an attempt to extend this concept and use the supplemental heater to actively control thruster mass flow (and thus current) to a desired value. To this end, a manual bang-bang style control system was attempted wherein the thruster was alternately placed in hot and cold runaway. Results are shown in Fig. 10. In the experiment, the discharge current was initially increasing, indicating hot runaway. As the discharge current increased past 6 A the power to the anode heater was reduced from 450 W to 100 W to cool the anode and decrease the propellant flow rate. As the anode cooled the discharge current decreased indicating cold runaway. As the discharge current dropped below 6 A, the power to the anode heater was increased to 450 W to reheat the thruster and increase the mass flow rate and discharge current once more. This process was repeated to "stabilize" the discharge current to values within the vicinity of 6 A. After four cycles the power limits on the heater were adjusted to reduce the oscillation amplitude in the discharge current. The lower power limit was changed to 150 W and the upper limit was changed to 350 W. This successfully reduced the peak-to-peak amplitude of the current oscillations from ~1 A to less than 0.5 A.

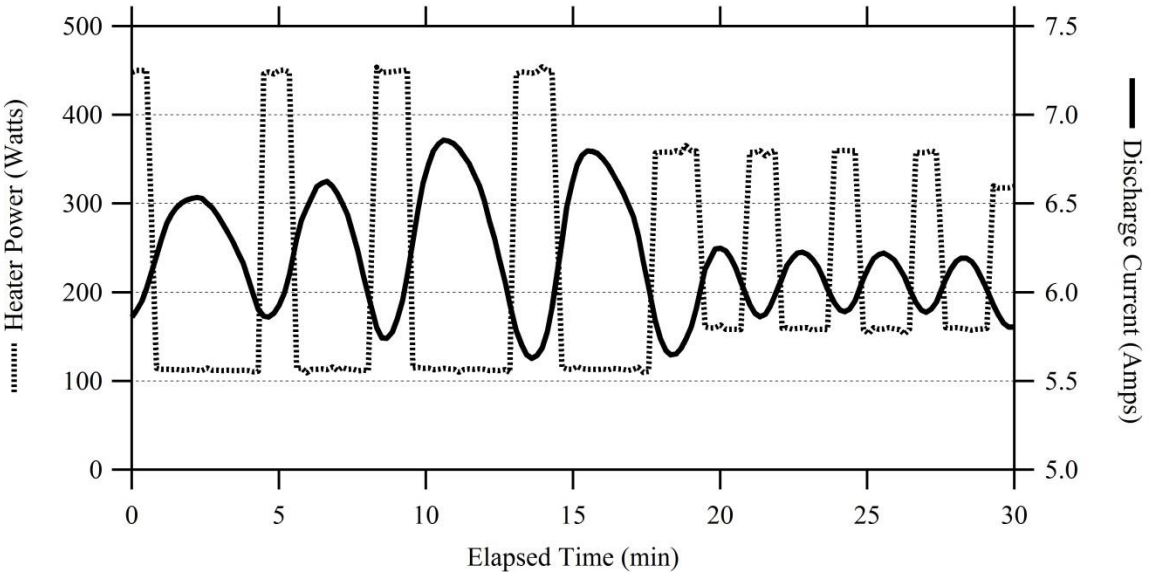

Fig. 10. A graph demonstrating a manual bang-bang control system that alternatively places the thruster in hot and cold runaway. As the discharge current increases past 6 A the power to the anode heater is reduced. As the anode and subsequently the propellant cools the discharge current decreases. Once the discharge current falls below 6 A the power to the anode heater is increased, heating the propellant and increasing the mass flow rate. Decreasing the high power limit and increasing the lower power limit of the bang-bang scheme at 18 minutes reduced the amplitude of the current oscillations. The discharge voltage was constant at 300 V and the current to the electromagnets was a constant 2.3 A.

3.4. Automated Control Tests

The results of the manual bang-bang control system test showed that the anode heater could control the inherently unstable direct evaporation system; however the test permitted discharge current variations of 0.5 A. In order for the control system to be viable as a flight control system, the control process must be automated, so a simple software proportional, integral, derivative (PID) control system was developed that used the discharge current as the measured, or process, variable and the current supplied to the anode heater as the control variable. The PID control equation is shown below in

equation (9) where $I_{AnodeHeater}$ is the current supplied to the anode heater, K_c is the proportional gain, T_i is the integral time, T_d is the derivative time, and ε is the difference between the desired discharge current set point and the measured discharge current.

$$I_{AnodeHeater} = K_c \left[\varepsilon + \frac{1}{T_i} \int \varepsilon dt + T_d \frac{d\varepsilon}{dt} \right] \tag{9}$$

LabVIEW™ software was used in conjunction with data acquisition hardware to measure and control the output of the power supplies controlling the thruster anode and anode heater. The program measured the discharge current of the thruster and used equation (9) to set the output current of the anode heater. This measurement and calculation occurred at a frequency of 1 Hz.

The PID loop was manually tuned. The proportional gain was determined through several guess-and-check experiments while the effect of changing the integral and derivative times is shown in Fig. 11. The controller performance was evaluated by commanding step changes in the discharge current and monitoring the dynamic response of the system. For each set of gains the first set point was 6 A and then after several damped oscillations the set point was commanded to 7 A and allowed to settle again. Once a few damped oscillations occurred at the higher set point the PID gains were then changed and the set point was reduced to 6 A to start a new cycle. The results of the experiment showed that the lowest settling time was achieved with the second set of gains tested: $K_c = 10$, $T_i = 3.00\,\text{min}$, and $T_d = 0.01\,\text{min}$.

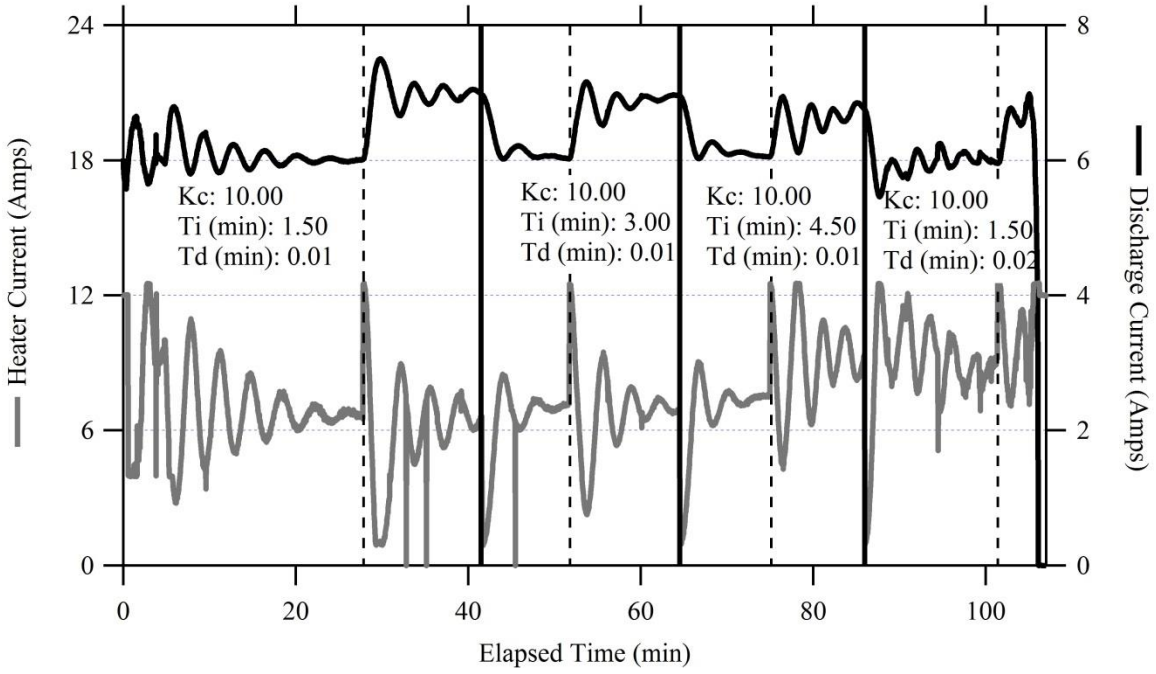

Fig. 11. A graph illustrating the effect of PID gains on settling time. The set point for the discharge current is alternated between 6 A and 7 A. The vertical dashed lines in the graph indicate the times where the set point changed from 6 A to 7 A. The solid vertical lines occur at times where the set point was reduced from 7 A to 6 A. The PID gains were also changed at the time indicated by the solid vertical lines.

Once the PID gains were chosen longer duration tests were performed to test the stability of the system. These tests were successful for discharge current set points below 7 A. At higher currents the oscillations in the discharge current were no longer damped with the gains as described above. This was rectified by one final change in the PID parameters. The derivative gain was increased by 600% to $T_d = 0.06\,\text{min}$ forcing extra damping on the system. This extra damping eliminated the oscillations in the discharge current at all values of set point that were tested. The results of the experiment are shown in Fig. 12.

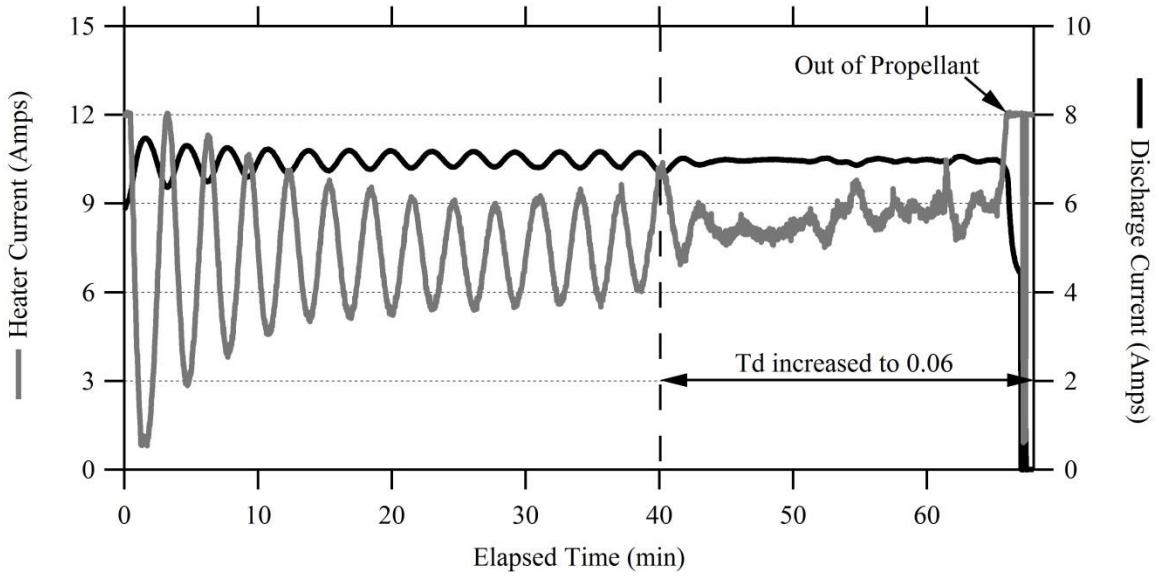

Fig. 12. The results of a long-duration test with a discharge current set point of 7 A. For the first 40 minutes of the test the PID parameters were Kc = 10, Ti = 3.00 min, Td = 0.01 min. At 20 minutes, however, the oscillations in the discharge current reached steady state and were no longer damped. At 40 minutes the derivative time, Td, was increased to 0.06 min, at which point the current immediately settled on the set point.

To optimize Hall thruster performance at a given discharge voltage and mass flow it is necessary to tune the electromagnets such that the discharge current is minimized. In order to find the optimum magnet current, the discharge current was monitored as the current to the electromagnets was swept between 2.5 A and 2.1 A. Because the discharge conditions are slightly coupled to the mass flow rate of the thruster (e.g. changing discharge current will alter the total heat load to the anode) the PID control system was first turned off and the electromagnet current was swept quickly such that the thruster thermal response was negligible. The results of the test are plotted in Fig. 13 and show that the optimum electromagnet current was 2.18 A.

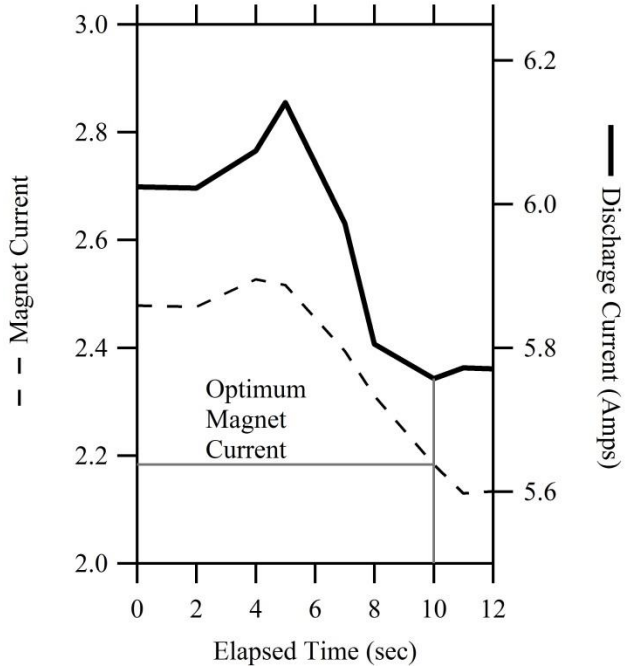

Fig. 13. The electromagnet current was swept between 2.5 A and 2.1 A while recording the discharge current. The minimum discharge current occurred at 10 s, corresponding to an electromagnet current of 2.18 A. The discharge current was held at a constant 300 V and the anode heater power was held at 130 W.

3.5. Thrust Data

Thrust data were obtained using the automated PID control system during two tests: Test 1 and Test 2. The thrust stand was a NASA-Glenn style, inverted pendulum, null-displacement thrust stand. For Test 1, the thruster was operated at 300 V discharge with a discharge current set point of 6 A. The data obtained from the test are plotted in Fig. 14. The graph in Fig. 14 shows the un-altered data from the experiment in its entirety. At 2 minutes into data collection the pre-heat was initiated. Unfortunately due to a malfunction in the anode heater power supply, the anode heater voltage was not recorded so only heater current data (and not heater power) are available. The anode potential was set to 300 V during the pre-heat and the magnet current was varied between 0 and 0.8 A.

After 25 minutes of pre-heat the thruster ignited. The magnet current was then slowly increased to 2.15 A, driving the thruster into voltage-limited operation at 300 V discharge. Once the thruster was voltage limited, at 27 minutes, the PID controller was turned on with a discharge current set point of 6 A and the thruster control was automated for the rest of the experiment. The results of Test 1 showed that the thruster produced ~44 mN of thrust after eliminating the linear thermal drift in the thrust measurement. This thrust measurement yields a thrust-to power of 24.4 mN/kW.

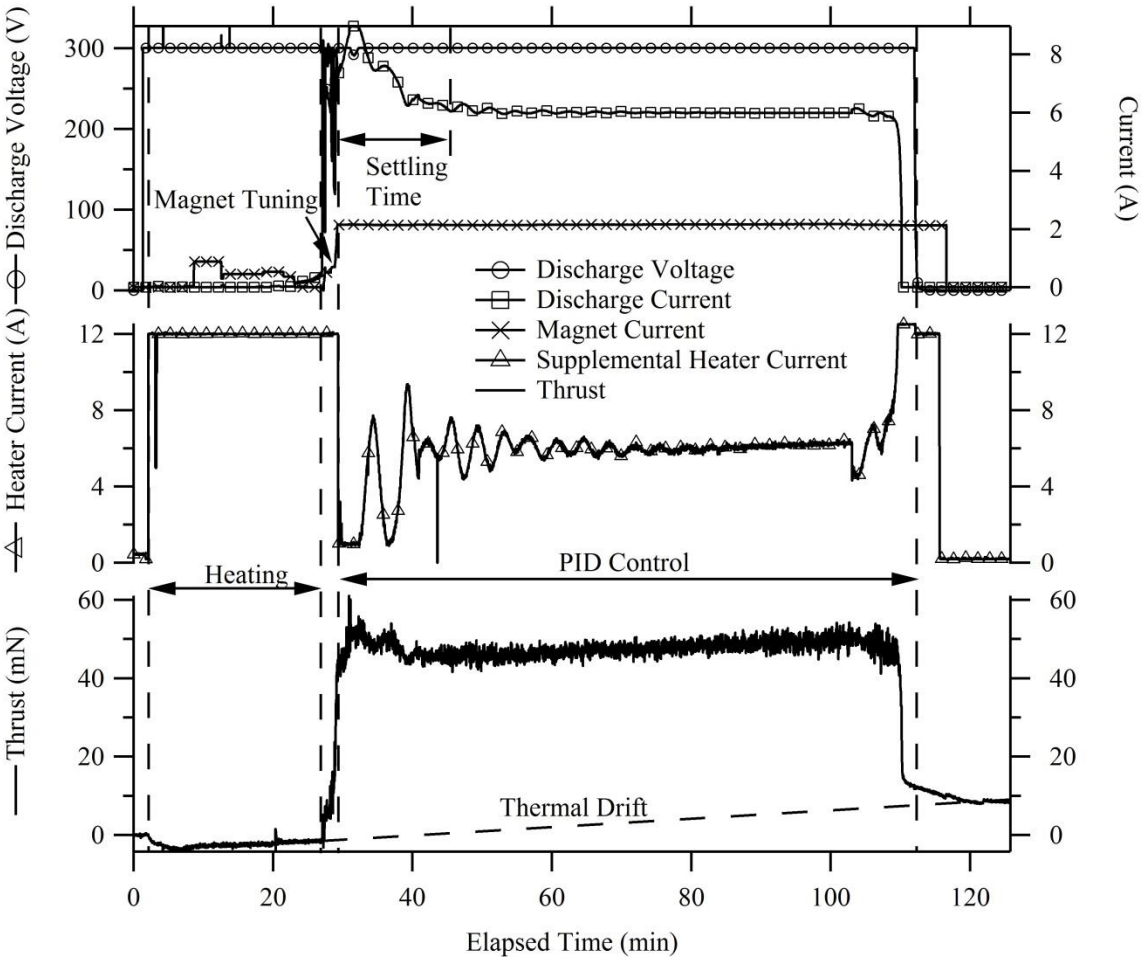

Fig. 14. The results from Test 1. The thruster was first pre-heated for 25 minutes with the anode potential set to 300 V. Once the discharge was established, the magnets were tuned and the PID loop was turned on at 27

minutes to a set point of 6 A. The discharge current settled within 15 minutes and thrust data were recorded for the duration of the test.

Test 2 was similar to Test 1. The thruster was again operated at 300 V but at a discharge current set point of 7 A. The results of Test 2 are plotted in Fig. 15 starting once the PID controller was engaged. Unlike Test 1, in Test 2 the power provided by the anode heater was known and recorded. Once the discharge current settled the power supplied by the anode heater oscillated near 136 watts; only ~6% of the total system power is used in the anode heater. Thrust data were also obtained. As with Test 1 there was a linear thermal drift in the thrust data. Accounting for the thermal drift yields ~50 mN of thrust and a corresponding thrust-to-power ratio of 23.8 mN/kW, which agrees well with the thrust-to-power of 24.4 mN/kW found in Test 1.

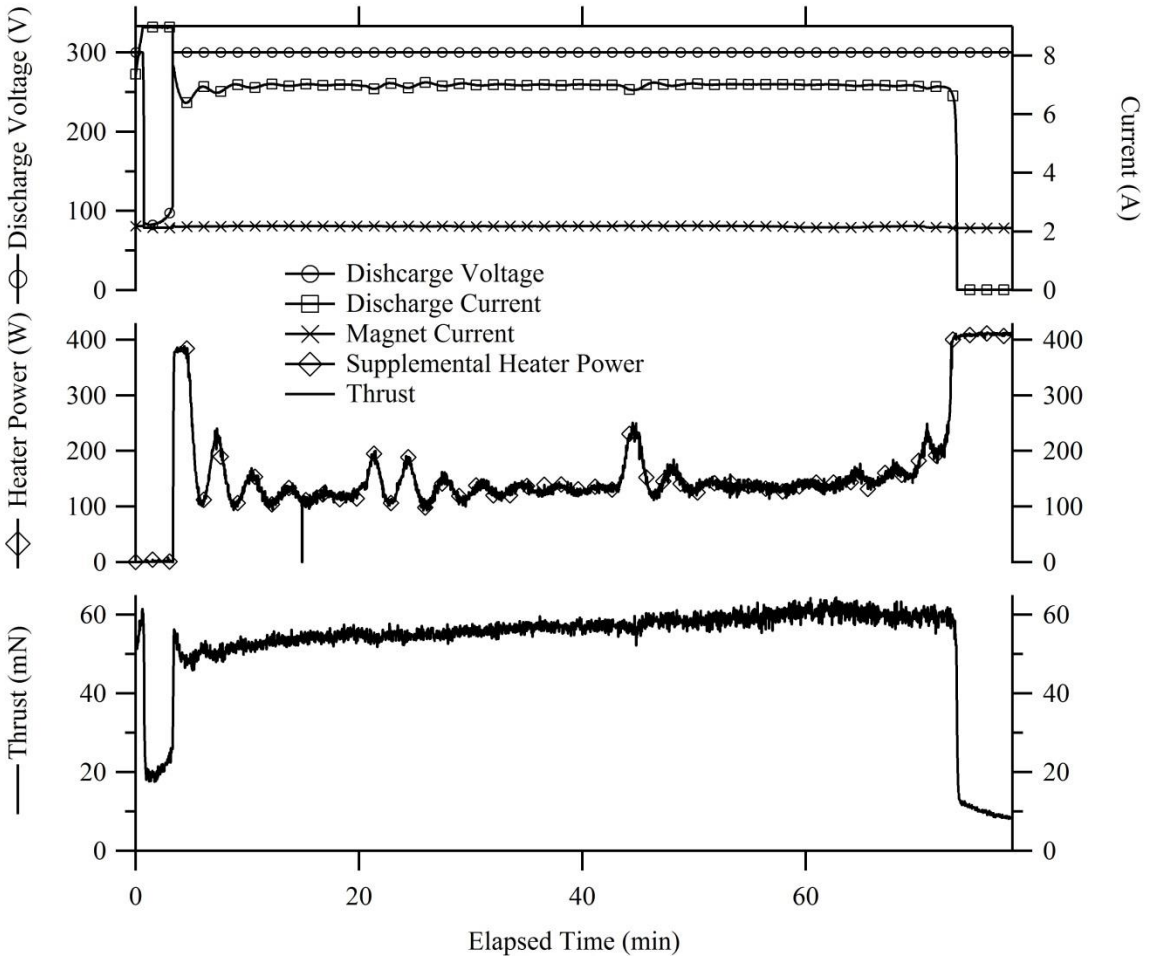

Fig. 15. The results of Test 2. For the entire test the thruster was operated voltage limited except for a short period of current-limited operation at the beginning while the PID controller converged. As the discharge current approached the set point, the anode heater power settled near 136 W, representing only 6% of the total power to the thruster. As with Test 1, there was a linear drift in the thrust data. Accounting for the drift yields a thrust of ~50 mN and a thrust-to-power of 23.8 mN.

3.6. Conclusion

By using the direct evaporation method supplemented with a heater located behind the anode, a thruster operating on magnesium propellant can be stably operated in constant-voltage mode. A PID control system was used to control the anode heater and automate the mass flow control system. It was found that during steady-state operation

the anode heater only required ~136 W of power and the mass flow control system only consumed 6% of the total system power. Multiple operating points were also demonstrated, and thrust data were obtained. With a discharge voltage of 300 V and a discharge current of 6 A, the thrust-to-power ratio was 24.4 mN/kW at 44 mN of thrust. Increasing the discharge current to 7 A showed a thrust-to-power ratio of 23.8 mN/kW at 50 mN of thrust.

Chapter 4

Performance Comparison between a Magnesium- and Xenon-fueled 2 kW Hall Thruster[2]

One of the most important metrics in the evaluation of magnesium propellant is the performance of a thruster using magnesium compared to the performance using xenon. Theoretically, it should be possible to achieve very high specific impulses (~4000 s) at relatively low voltages (300 V) using magnesium propellant. For the best evaluation of the performance of the propellant, xenon and magnesium should be tested using as much of the same thruster hardware as possible.

4.1. Goal of Study

The goal of this study was to measure the performance of a 2-kW Hall-effect thruster modified to operate on magnesium vapor using active thermal mass flow control and to compare the magnesium performance to that demonstrated using xenon propellant. Sections 4.2 and 4.3 describe the thruster, test equipment, and experimental methodology. Section 4.4 reports the thrust, specific impulse, thrust-to-power, and efficiency of magnesium propellant obtained at several operating points. Section 4.5 reports the results

[2] The contents of this chapter have been submitted in an article to the AIAA Journal of Propulsion and Power coauthored by Mark A. Hopkins and Lyon B. King.

of two experiments using xenon propellant: performance of the thruster with the anode heater turned off and performance of the thruster after being heated in the same manner as the magnesium-fueled thruster. Section 4.6 discusses the results and compares the magnesium performance to the xenon performance.

4.2. Description of Apparatus/Experimental Methods

All of the experiments reported here were performed in the Ion Space Propulsion Laboratory at Michigan Technological University. Xenon experiments were performed in the Xenon Test Facility—a 2-m-diameter, 4-m-long vacuum facility evacuated using two cryogenic pumps with a combined pumping speed of 120,000 liters-per-second of nitrogen for a base pressure of 10^{-6} Torr. Experiments using magnesium propellant were performed in the Condensable Propellant Facility (CPF). The CPF is a 2-m-diameter, 4-m-long vacuum facility evacuated using three turbomolecular pumps with a combined pumping speed of 6,000 liters-per-second on nitrogen for a base pressure of 10^{-5} Torr.

The thruster used for these experiments was a laboratory thruster based on the Aerojet BPT 2000, which was intentionally designed for operation on xenon. A custom LaB_6 laboratory hollow cathode was used to sustain the discharge. For experiments using xenon propellant, the cathode was operated using a 1 mg/s flow of xenon. For experiments using magnesium propellant, the cathode was operated using 0.3 mg/s of argon gas. The magnetic circuit of the BPT 2000 was preserved but the anode was modified for use with magnesium and a supplemental heater was installed behind the anode. Rather than using a tungsten heater (as was used previously), a graphite heater was cut from carbon paper and sandwiched between two boron nitride insulative discs

isolating the heater from anode potential. The carbon heater had significantly longer life than the tungsten heaters and maintained flexibility even after multiple thermal cycles. The windings of the resistive heater were counter-wound to minimize disturbance to the magnetic field topography. The anode used was described in detail in Hopkins and King [55] and has an open area of 14.8 x 10^{-6} m^2. Figure 16 shows a section view of the Hall thruster geometry and highlights the major components.

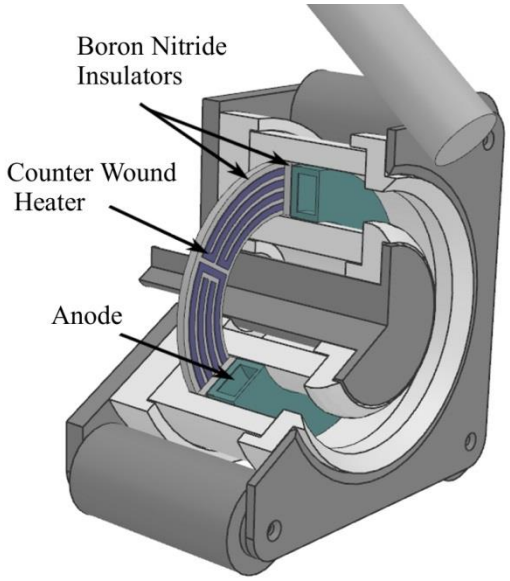

Fig. 16. A section view of the Hall thruster showing the configuration of the anode and supplemental heater.

All thrust measurements were obtained using a NASA-Glenn style [57] inverted pendulum null-displacement thrust stand similar to that fabricated by Xu and Walker [58] and capable of measuring thrust to within ±1 mN. Calibration of the thrust stand was performed after lighting the cathode to eliminate thrust enhancements from the cathode. When measuring magnesium performance, thruster calibration was performed after partially heating the thruster to minimize thermal drift in the thrust measurements.

Six thruster tests were performed using magnesium propellant. For each thruster test using magnesium, the same heating procedure was used to maintain consistency. The

thruster magnet current was set to 0.4 A to minimize glow discharge during thruster outgassing. With the thruster at room temperature a discharge was created between the cathode and a keeper electrode. The cold anode was biased to 300 V with the discharge power supply current limit set to 9 A. An automated heating profile then pre-heated the thruster. The profile increased the current on the supplemental heater by 1 A every seven minutes from 0 A to 11 A with one exception: upon reaching 8 A the program maintained constant heater current for 45–50 min while the thrust stand was calibrated, after which the profile resumed the 1 amp-per-seven-minutes rate. After the thrust stand was calibrated the magnet current was decreased to 0.0 A to allow the thruster to ignite. Once the anode reached sufficient temperature for propellant vaporization the thruster discharge would spontaneously ignite and instantly hit the current limit of 9 A with the discharge voltage falling below the 300 V pre-set. While still current limited, the voltage limit of the power supply was set to 200, 250, or 300 V depending upon the experiment, and the electromagnet current was increased to nearly the optimum value (known a priori based on past testing). The automated PID control system—outlined in Hopkins and King [55] and Chapter 3 of this document—was then enabled and used to control the supplemental heater to achieve the desired discharge current (mass flow rate). After initiating the control system, a software PID loop reads the discharge current and adjusts the current sent to the supplemental anode heater. The proportional gain used was $K_c = 8$, the integral time was $T_i = 3.00$ min and the derivative time was $T_d = 0.09$ min.

4.3. Measuring the Mass Flow Rate of Magnesium

Figure 17 shows the telemetry of a typical thruster test from beginning to end indicating four distinct phases: heating, transition, stable operation, and cooling. The mass flow rate must be determined by comparing pre- and post-test weights of the thruster assembly. This technique will give a measure of the total propellant consumption of the entire test, including propellant that was expelled during heating, transition, stable operation, and cooling phases. In order to evaluate the thruster performance during the stable operation period we must correct this measurement to account for the propellant lost during heating, transition, and cooling. This section describes the method by which the mass flow rate is determined for the stable operation portion of the thruster test.

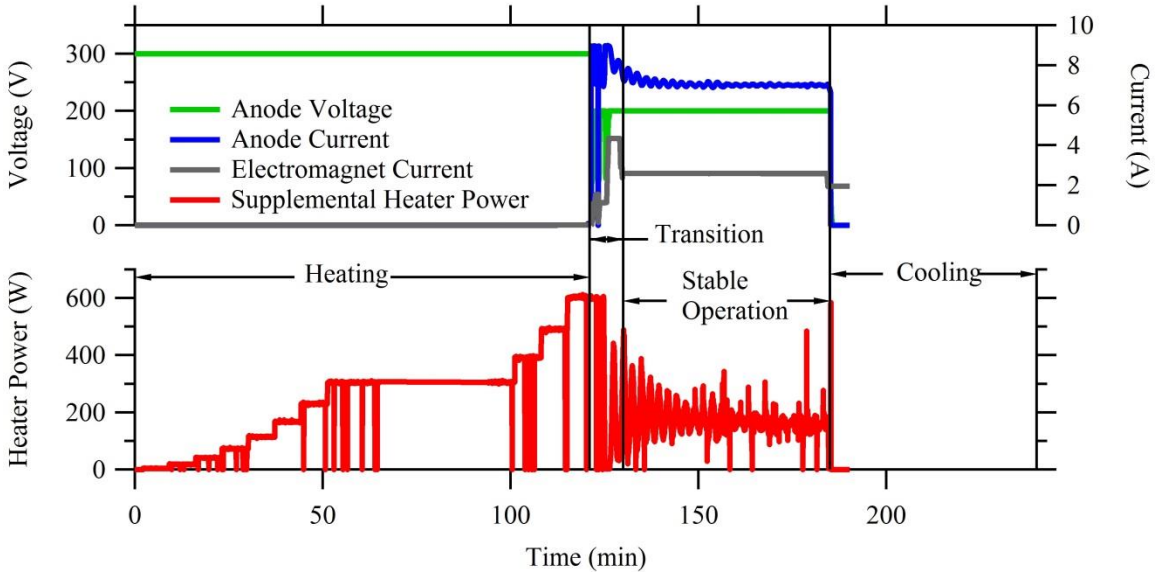

Fig. 17. Telemetry from an entire thruster test using magnesium highlighting the four portions of a magnesium test: heating, transition, stable operation, and cooling.

Because the heating profile is automated and repeatable, and also because the cooling phase should be identical from test-to-test, we assume that the propellant mass lost during these two phases is similar for every performance experiment. The transition period, however, is not controllable and is different for each test. We measure the total heating,

transition, and cooling losses in dedicated tests—henceforth referred to as 'startup tests'—wherein the thruster is heated, ignited, allowed to transition, and then cooled with zero seconds of stable operation. Subtracting the heating, transition, and cooling propellant mass loss, as measured from these dedicated tests, from the total mass loss measured during a performance experiment—such as that shown in Fig. 17—gives the mass used during the stable operation phase of the performance experiment.

Of the four phases of a magnesium test, the mass flow rate of the thruster was highest during the transition phase. This is supported by the thruster operating with the power supplies current limited at 9 A with voltages as low as 100 V for several minutes. Because the mass flow rate during transition phase is significantly higher than the mass flow rate of the other three phases of the test, it is the effect of the transition phase that must be precisely accounted for when correcting to determine the mass flow rate of the stable operation. To calculate the adjusted mass flow rate—that is, the mass flow rate adjusted to remove heating, transition, and cooling losses—we start by measuring the total mass of propellant lost in a startup test and the transition time—the total amount of time the discharge current was greater than 1 A. We then subtract the total mass lost from the startup test from the total mass of a full-length performance test yielding the adjusted mass of the performance test.

Because the duration of the transition period varies from test to test, it is not sufficient to divide the adjusted mass lost by the time period of stable operation for the performance test to calculate stable mass flow rate. Figure 18 shows a graph of the telemetry of a 'startup test' in its entirety. The mass lost during the experiment was 1.2 g and the transition portion of the test was 433 s. The mass lost in the experiment whose telemetry

is graphed in Fig. 17 was 7.3 g, the time period of stable operation was 3481 s, and the transition period was 345 s. The adjusted mass lost from the test in Fig. 17 is 6.1 g. Dividing the adjusted mass by the time period of stable operation gives a mass flow rate of 1.75 mg/s. If instead of dividing the adjusted mass lost by the time period of stable operation, we divide the adjusted mass lost by the total operation time minus the transition time we take into account the difference in the difference in transition time between the startup test and the full-length performance test. Doing so yields a mass flow rate of 1.79 mg/s—closer to the actual mass flow rate of the thruster.

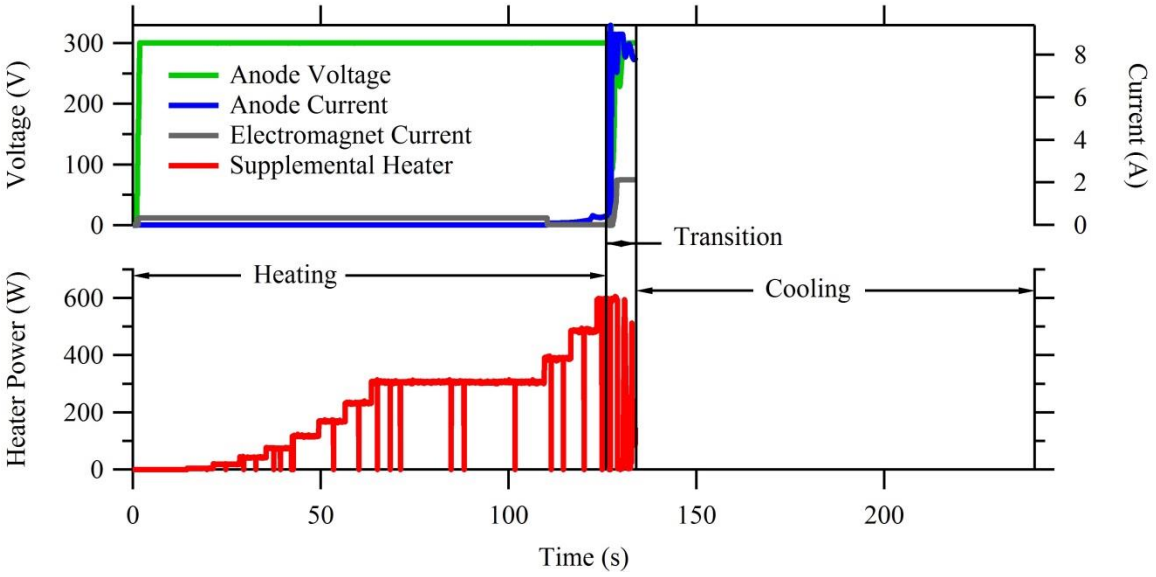

Fig. 18. A graph showing the telemetry for a startup test.

4.4. Magnesium Performance

In this section the performance of the magnesium fueled thruster was obtained at several operating conditions. For each test, the thruster was started using the procedure outlined in Section 4.2. After the thruster stabilized at the desired anode voltage and anode current, the electromagnet current was tuned to minimize the discharge current.

Due to the nature of the thermal control system, tuning the electromagnets must be done thoughtfully: changing the electromagnet current affects the discharge current, which changes the thermal load on the anode, which affects the mass flow rate. Because of this, the electromagnets must be adjusted on a timescale fast with respect to the thermal response time of the anode so that the mass flow rate remains constant [18,55] and a true optimum electromagnet current can be identified.

Before evaluating the performance of the thruster, the mass flow rate as a function of discharge current must be measured. Using the methods outlined in Section 4.3, three adjusted mass flow rates can be calculated for each performance test—one adjusted mass flow rate for each of the startup tests. Because there were three performance tests recorded using a 7 A discharge current, there are nine calculated adjusted mass flow rates. Because there was only one performance test at 5 A discharge current there are three calculated adjusted mass flow rates. Taking the mean and standard deviation of the nine adjusted mass flow rates for a 7 A discharge yields a mean adjusted mass flow rate of 1.73±0.06 mg/s. Taking the mean and standard deviation of the three adjusted mass flow rates for the 5 A current yields 1.02±0.09 mg/s. The important characteristics of these tests—the total duration of the test and the propellant mass lost—are tabulated in Table 1.

Table 1. Tabulated propellant usage for full-length performance tests and heating and cooling tests.

Test Type	***Total* Mass Lost**	***Total* Duration**
Startup	1.9 g	859 s
Startup	1.9 g	635 s
Startup	1.2 g	433 s
7 A Performance	7.3 g	3826 s

7 A Performance	6.9 g	3741 s
7 A Performance	10.5 g	5705 s
5 A Performance	3.7 g	2618 s

The thruster was operated at several discharge conditions: 200 V at 7 A, 250 V at 7 A, 300 V at 7 A, and 300 V at 5 A. At each of these conditions several performance measurements were obtained in real time including: anode voltage, anode current, supplemental heater voltage, supplemental heater current, and thrust. Reported values of anode current, supplemental heater power, and thrust are those measured during the stable operation portion of the thruster test as defined in Section 4.3. Additionally the propellant mass used during each experiment was recorded along with the total operating time—defined as the total time the discharge current was greater than 1 A—which were used to determine the mass flow rates calculated above.

First, the operating conditions of the thruster are examined. The anode current, adjusted mass flow rate, and anode voltage are shown in Table 2 and the supplemental heater power is plotted versus anode power in Fig. 20. The low variation of the anode current (less than 1% in all cases) demonstrates the reliability of the control system. A graph of the stable operation portion of a typical test is shown in Fig. 19 showing the stability of the control system. As expected the overall mass flow rate for each test was heavily dependent on the discharge current: each of the tests with a 7 A discharge used 1.73 ± 0.06 mg/s. The 5 A discharge case used considerably less mass flow, 1.02 ± 0.09 mg/s. Just as the mass flow rate correlated well with the discharge current, the supplemental heater power followed the discharge power. As the power at the anode increased, the supplemental heater power needed to maintain the desired propellant flow

rate decreased. The decrease in supplemental power with discharge power is expected because mass flow rate should be proportional to the combination of the discharge power and supplemental heater power. While the amount of supplemental power needed was upwards of 10% of the total system power (and as low as 2%), it has been discussed elsewhere [55] that the amount of supplemental power needed can be greatly reduced by optimizing the open area of the anode. Such optimization was not performed for these experiments, and so the efficiency values reported here do not include heater power.

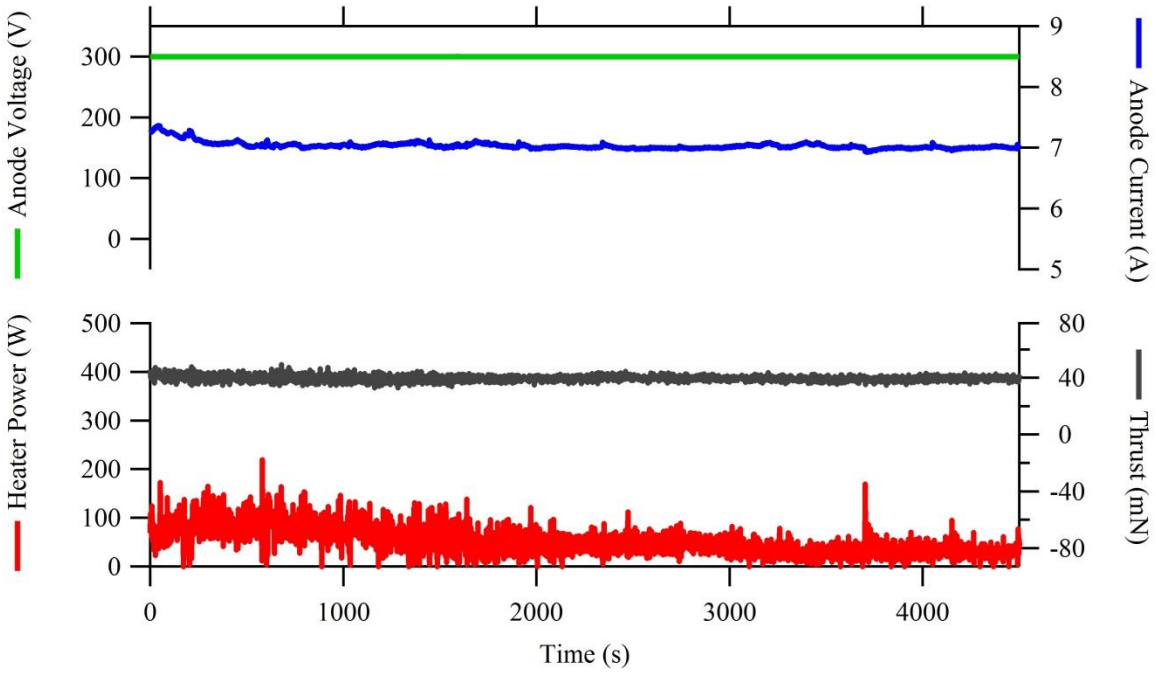

Fig. 19. A graph showing the anode voltage and current, thrust, and supplemental heater power during the stable operation portion of a full-length performance test.

Table 2. Tabulated thruster telemetry using magnesium propellant.

Anode Voltage	Anode Current	Adjusted Mass Flow Rate
200 V	7.01±0.03 A	1.73 ± 0.06 mg/s
250 V	7.01±0.04 A	1.73 ± 0.06 mg/s
300 V	7.02±0.03 A	1.73 ± 0.06 mg/s
300 V	5.02±0.04 A	1.02 ± 0.09 mg/s

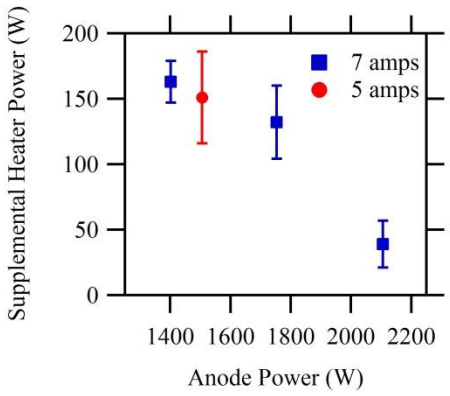

Fig. 20. Supplemental heater power plotted versus anode power. As thruster power is increased, the amount of supplemental power needed to sustain discharge decreases.

The thrust of the magnesium-fueled thruster is plotted versus anode voltage in the left graph in Fig. 21 where the error bars represent one standard deviation in the measured thrust. The thrust ranged from 34 mN at 200 V to 39 mN at 300 V for the 7 A discharge current tests. For the 300 V, 5 A condition the thrust was 27 mN. The thrust-to-power ratio, plotted versus anode voltage in the right graph shown in Fig. 21, shows the expected trends: thrust to power decreases with increased anode voltage, 24 mN/kW at 200 V to 18 mN/kW at 300 V, and increases with discharge current.

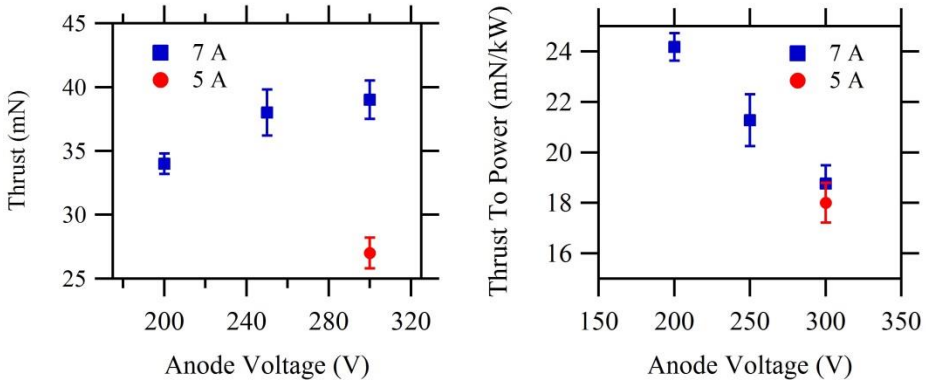

Fig. 21. Left: Measured thrust using magnesium propellant plotted versus anode voltage. Right: Thrust to power versus anode voltage for magnesium propellant. The thrust-to-power ratio decreases with discharge voltage as expected.

Specific impulse was calculated using the equation $I_{sp} = T/(\dot{m}g)$ where T is measured thrust, and $\dot{m}$ is the mean adjusted mass flow rate. Anode efficiency, η, was calculated using the equation $\eta = T^2/(2\dot{m}P^2)$ where P is the anode power (anode voltage multiplied by anode current). The left graph of Fig. 22 shows the calculated specific impulse and anode efficiency as a function of anode voltage. In the graphs, markers represent calculations using the mean adjusted mass flow rate and the error bars represent both the variation in acquired data and the variation in mass flow rate. As expected the specific impulse increases with anode voltage, from 2000 s at 200 V to ~2500 s at 300 V. Anode efficiency stays fairly consistent across all cases at ~23% with a slight decline with discharge voltage.

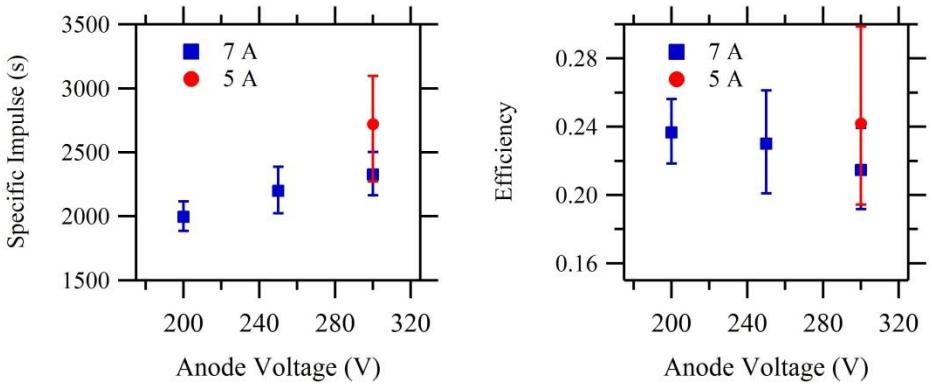

Fig. 22. Left: Specific impulse is plotted versus discharge voltage. Right: Efficiency plotted versus anode voltage. Error bars represent both higher and lower mass flow rates as well as variation in measured data.

4.5. Xenon Performance

Two experiments were conducted to measure the thruster's performance on xenon. The same hollow anode used for the magnesium tests was modified to include a feed tube to deliver xenon, but no other modifications were made to the anode or the supplemental heater system. For experiment (1), the performance of the thruster was measured with the supplemental heater powered off. For experiment (2), the same pre-heat profile used for magnesium testing was applied to the thruster and the supplemental heater was also powered during testing. For both experiments the thruster was mounted to the NASA-Glenn style, inverted-pendulum, null-displacement, thrust stand and operated using a laboratory cathode with 1 mg/s of xenon.

In experiment (1), the thruster was operated using 5 mg/s of xenon supplied to the anode. Thruster discharge was ignited at 300 V and the electromagnets were tuned to minimize the discharge current. After the thruster conditions stabilized (approximately 30 minutes) performance measurements were recorded: thrust was measured to be 76±1.5 mN, specific impulse was measured to be 1550±30 s, thrust-to-power was measured to be

53.5±1 mN/kW, and efficiency was measured to be 40±2%. The tabulated performance data from experiment (1) can be found in Table 3. It should be noted that the xenon efficiency of this particular thruster is significantly lower than state-of-the-art devices as confirmed previously by Sommerville in his work with the same thruster design [59].

The purpose of experiment (2) was to assess whether the elevated temperatures used during magnesium tests or the current through the supplementary heater affect thruster performance. In experiment (2) the thruster was heated using the supplemental heater in the same manner as the magnesium tests. Because the ignition of the thruster was not dependent on the temperature of the anode, the thruster discharge was ignited on 5 mg/s of xenon at 300 V discharge once the supplemental heater was at 11A for 5 min. The supplemental heater was then set to add 300 W of power to the thruster to simulate the hottest operation of the magnesium-fueled thruster. Performance data were then obtained: 76±1 mN, specific impulse was measured to be 1550±20 s, thrust-to-power was measured to be 55.4±1 mN/kW, and efficiency was measured to be 42±1%. The tabulated performance data from experiment (2) can be found in Table 3.

Table 3. Tabulated performance data using xenon propellant. Experiment 1 was performed with the supplemental heater turned off, and Experiment 2 was performed after heating the thruster in same manner as the magnesium thruster.

	Anode Voltage (V)	Mass Flow Rate	Anode Current (A)	Thrust (mN)	Specific Impulse (s)	Thrust-to-power (mN/kW)	Anode Efficiency
Exp. 1	300	5 mg/s	4.74	76±1.5	1550±30	53.5±1	40±2 %
Exp. 2	300	5 mg/s	4.57	76±1	1550±20	55.4±1	42±1 %

4.6. Comparison of Magnesium to Xenon Performance and Discussion of Results

The performance of the BPT 2000 as obtained through experiment (1) using xenon propellant was compared to the performance of the magnesium-fueled BPT 2000 operated at 300 V 5 A. The discharge conditions for the magnesium case and the xenon case are similar, but more importantly the molar flow rates of the propellants are matched within the error bars of the magnesium flow rate—5 mg/s xenon is the molar equivalent to 0.93 mg/s of magnesium, such that quantitative comparisons can be made. The thrust and thrust-to-power when operated using xenon were substantially higher than when operated using magnesium, 76 mN (53.5 mN/kW) compared to 27 mN (18 mN/kW), which is expected due to the much higher mass of xenon. Similarly, the specific impulse of the xenon thruster was substantially lower than that of the magnesium thruster: 1550 s compared to 2700 s. The efficiency of the xenon thruster was 40% while the magnesium thruster only had an efficiency of 23%. The low efficiency when operated on magnesium is most likely attributable to thruster design rather than to intrinsic inferiority of magnesium as a propellant. Plasma beam properties and analysis of the thruster design are considered in Chapter 5.

4.7. Conclusion

The performance of a 2-kW-class thruster was measured using magnesium propellant. The mass flow rate of the thruster was determined using a time-averaged total mass loss technique that was adjusted to account for evaporation during heating and cooling. The thruster was found to have a thrust-to-power ratio of 24 mN/kW to 18 mN/kW from 200 V to 300 V anode potential. The specific impulse was found to be 1900 s to ~2500 s from 200 V to 300 V anode potential. The anode efficiency of the magnesium thruster was

found to be 23% compared to 40% when operated using xenon propellant. The efficiency losses are likely due to the thruster being designed for xenon propellant, rather than magnesium.

Chapter 5

Magnesium Plume Properties and Comparison to Plasma Plumes from Other Propellants

Research concerning the ionization and acceleration regions are presented in this chapter. In order for the thruster to operate properly, certain plasma conditions must be created in the ionization and acceleration region: (1) there must be sufficient populations of electrons at proper energy to ionize the working gas; (2) the electron-neutral collision frequency must be sufficiently high in the ionization/acceleration region of the Hall thruster channel. These two requirements are achieved when a thruster's physical dimensions, electric field, and magnetic field are designed appropriately. From Kim [2] and Katz and Goebel [39] we know that the ionization mean free path, λ_i, shown in equation (10), dictates the necessary length of the Hall thruster discharge channel and ionization/acceleration region for proper ionization and acceleration of ions.

$$\lambda_i = \frac{v_n}{n_e \langle \sigma v_e \rangle} \tag{10}$$

In equation (10) v_n is the neutral velocity in the axial direction; n_e is the electron number density; σ_i is the ionization cross section of the neutral atom at a given electron energy, v_e; and $\langle \sigma v_e \rangle$ is the ionization rate coefficient. In order to have significant ionization of

the working gas the axial length of the ionization/acceleration region, L_i, must be much larger than the ionization mean free path:

$$\frac{\lambda_i}{L_i} \ll 1. \tag{11}$$

The relations in equations (10) and (11) indicate there are several control parameters in the design of a Hall thruster discharge channel: (1) electron temperature—controlled through discharge potential and channel dimensions [60,61], (2) thickness and location of ionization/acceleration region—controlled by channel dimensions [61-64], magnetic field topology and discharge potential [40], and neutral flow rate [65,66]. The biggest implication of equation (11) is that different propellants may require physically different thruster dimensions to achieve the same efficiencies at the same operating parameter. Studies using krypton [59] and magnesium propellant in a BPT 2000 Hall thruster showed that simply changing the propellant dropped the thrust efficiency by 20-30%.

5.1. Goal of Study

The goal of this study was to examine plasma beam characteristics using several neutral species in a BPT-2000 Hall-effect thruster—magnesium, krypton, xenon, and bismuth—in order to identify loss mechanisms and suggest thruster scaling based on propellant species. For this study original experimental data were combined with the results of previous studies [15,59]. Data were obtained in the plasma plume of the same thruster operated using magnesium and xenon including measurements of plasma potential, electron temperature, electron density, off-axis current distribution, and ion energy distribution. Additionally, data from previous studies where off-axis current

distribution and ion energy were measured using krypton [59] and bismuth [15] propellant were compared to the data obtained using magnesium and xenon.

5.2. Description of Apparatus/Experimental Methods

The thrusters and facilities used in the experiments reported here were the same as those used in Chapter 4. Current density measurements were obtained using a Faraday probe consisting of a 2.5-mm-diameter tungsten rod sheathed in an alumina tube with an outer diameter of 4.75 mm. The probe was mounted on a rotational motion stage above the thruster and swept in an arc through the plasma beam at a radius of 250 mm. A bias of -20 V was applied to the probe with respect to ground—well below ion saturation—such that electrons were repelled from the probe. Ion current was measured using a 1 kOhm shunt resister as a function of angle with the thruster axis at 0 deg. A low pass filter with a time constant of 1 ms was used to filter high frequency noise from the current traces. The probe was swept at a speed of 7 deg/s such that the lag in the current reading was less than the angular resolution of the probe.

Ion energy characterization was performed using a retarding potential analyzer (RPA), shown schematically in Fig. 23. The electron repelling grids were held to -15 V, the ion-repelling grid was swept from 0-350 V, and the current collector was biased to -5 V—all with respect to ground. The probe was located 350 mm downstream from the thruster on the thruster axis. Current was measured using a μCurrent current amplifier with a low pass filter to filter out high frequency noise. The time constant of the filter was 100 ms, and the speed of the voltage sweep was approximately 6 s, such that the current change lagged the voltage change by 7 V. The current versus voltage sweeps were

adjusted to reflect the lag caused by the filter by shifting the current data by a time equal to two time constants (shifting -15 volts).

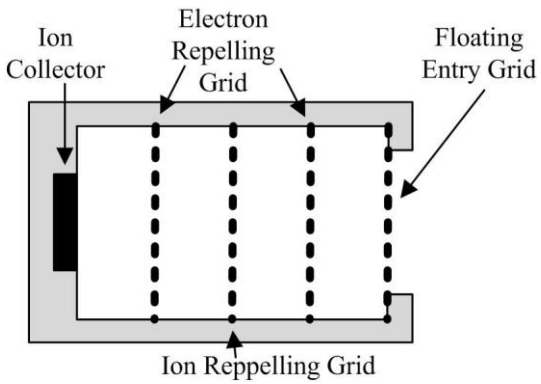

Fig. 23. Notional schematic of a retarding potential analyzer. Plasma enters through the floating grid. Electrons from the plasma are filtered out by the negatively biased (-15 V) electron-repelling grid. Ions are selectively filtered by energy using the positively biased ion repelling grid ranging from 0 V to potentials greater than the discharge potential. The ions that make it through the ion-repelling grid are collected on the ion collector, which is biased slightly negative. Ions striking the ion collector sometimes eject secondary electrons, which are suppressed by the electron-repelling grid near the collector—also biased to -15 V.

Plasma density, electron temperature, and plasma potential were measured using a double Langmuir probe. The probe consisted of two tungsten wires 0.7 mm in diameter protruding 4.6 mm from a double bore alumina tube sealed with alumina paste. A Keithley 2410 sourcemeter was used to measure the current flowing between the two tungsten wires as a function of the applied potential difference; the voltage was swept between -40 V and 40 V. The current-voltage traces were analyzed using a hyperbolic-tangent fit. The fit equation is shown in equation (12), where I is the current drawn between the probes; a_1 is the ion saturation current; a_2 is related to the electron temperature; and a_3, a_4, and a_5 are used to fit the curve but not related to physical quantities.

$$I = a_1 \tanh\left(a_2\left(V - a_5\right)\right) + a_3 V + a_4 \tag{12}$$

Using a_2, the electron temperature, T_e, can be calculated using the equation:

$$T_e = \frac{e}{2k_B a_2} \tag{13}$$

The electron temperature, combined with the ion saturation current, a_1, can be used to determine the plasma density, n_e, using the equation:

$$n_e = \frac{a_1}{eA_p}\sqrt{\frac{m_i}{k_B T_e}}\,. \tag{14}$$

Plasma potential was calculated using the obtained value of electron temperature according to

$$V_p = V_f + \frac{k_B T_e}{2e}\ln\left(\frac{2m_i}{\pi m_e}\right) \tag{15}$$

where V_f is the floating potential, m_i is the atomic mass of the ions, and m_e is the mass of an electron.

5.3. Magnesium and Xenon Plasma Plume Properties at Matched Operating Conditions

For the experiments reported here, laboratory BPT 2000 Hall thrusters were operated on xenon and magnesium propellant. The thruster was operated with a discharge potential of 300 V and a discharge current of 4.8 A for xenon and 5.0 A for magnesium. The propellant flow rate was matched at the molar flow rate 5 mg/s of xenon and 1.02 ± 0.09 mg/s of magnesium (see Chapter 4). Three sets of data were collected and used to

compare the plasma characteristics of both a magnesium-fueled Hall thruster and a xenon-fueled Hall thruster. First, the general plasma properties—electron density, electron temperature, and plasma potential—were measured by a double Langmuir probe; second, the ion energy distribution function was measured using a retarding potential analyzer; and third, the distribution of beam current was measured as a function of off-axis angle using a planar faraday probe.

5.3.1. Plasma Properties—Density, Temperature, and Potential

Electron density, electron temperature, and plasma potential were measured using a double Langmuir probe. A hyperbolic fit was applied to the measured current-voltage characteristics from which the plasma parameters were derived. The process is explained in detail in Section 5.2. For both propellants, data were obtained in two linear sweeps downstream from the thruster from 160 mm downstream to 300 mm downstream: one set of data was taken in line with the thruster discharge channel, and one set of data was taken in line with the thruster axis. A schematic of the data collection points is shown in Fig. 24.

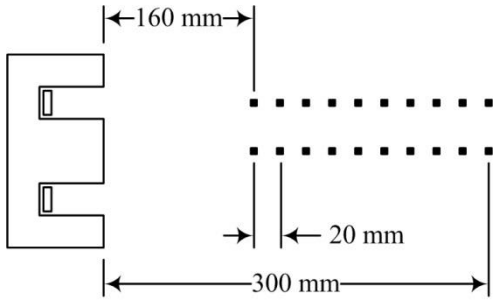

Fig. 24. Schematic showing the points at which Langmuir probe data were obtained.

First, an investigation of the electron temperature measured in both plasma plumes shows no significant trends. For both magnesium and xenon propellant, the electron

temperature is higher downstream of the thruster axis than downstream of the channel. There is a monotonically decreasing trend in the electron temperature for the xenon plasma, and no trend with distance for the magnesium plasma. However, the electron temperature for both propellants was between 2 eV and 4 eV. The electron temperature as a function of downstream distance from the face of the thruster is shown in Fig. 25.

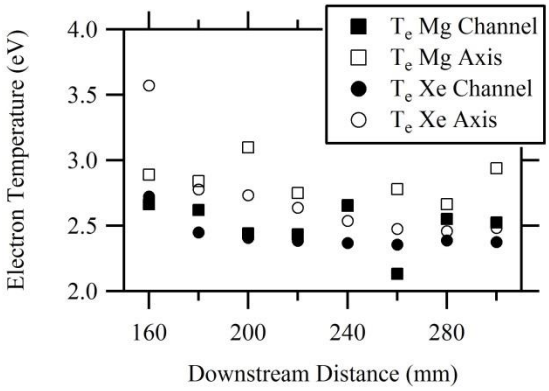

Fig. 25. Electron temperature measurements in magnesium and xenon plasma as a function of distance from the face of the thruster.

Investigations of the plasma potential with respect to facility ground reveal some more significant trends than the electron temperature. Again, the plasma potential of the xenon plasma was monotonically decreasing with distance from the thruster, and the plasma potential of the magnesium plasma remained fairly constant. However the plasma potential in the xenon plasma was higher than in the magnesium plasma at the same spatial locations. A graph of the plasma potential versus distance is shown in Fig. 26.

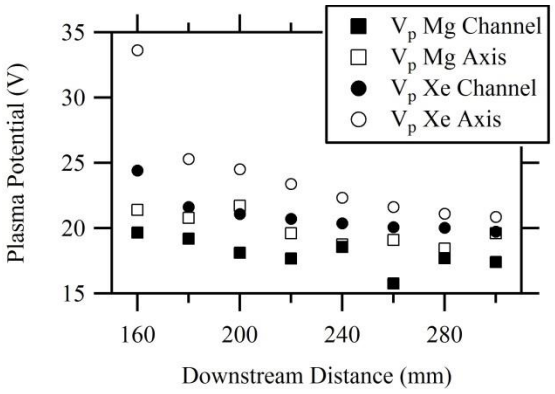

Fig. 26. The plasma potential with respect to ground for magnesium and xenon propellant as a function of downstream distance from the face of the thruster.

The biggest trend was seen during investigations of the plasma density. The plasma density for both magnesium and xenon propellant monotonically decreased as a function of distance from the thruster face. Additionally, there was an order of magnitude difference in the plasma density between the xenon plasma and the magnesium plasma in all spatial locations. Plasma density is plotted as a function of downstream distance from the thruster in the graph in Fig. 27.

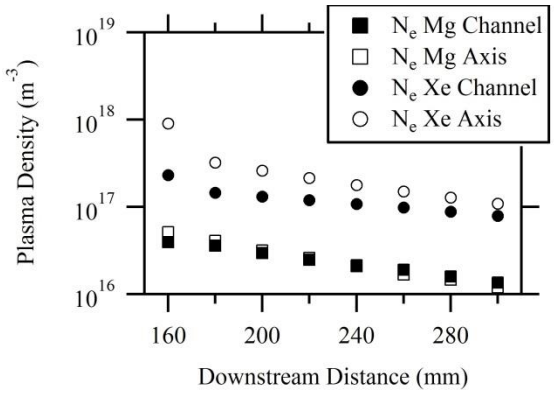

Fig. 27. Electron density for both magnesium and xenon plasma as a function of downstream distance from the thruster face.

5.3.2. Ion Energy

The ion energy distribution function was measured using a retarding potential analyzer in the plumes of both the magnesium-fueled thruster and the xenon-fueled thruster. The RPA was placed 320 mm downstream from the thruster face centered on the thrust axis. Plasma current on the collector electrode was measured as a function of retarding potential. The current-versus-retarding-potential traces are plotted in Fig. 28. From the traces it is readily apparent that the magnesium ions are retarded at much lower voltages than the xenon ions. At 100 V there is already a significant drop in ion current for the magnesium plasma case. It also appears that the xenon trace has a much sharper drop in ion current indicating a less widely distributed ion energy distribution.

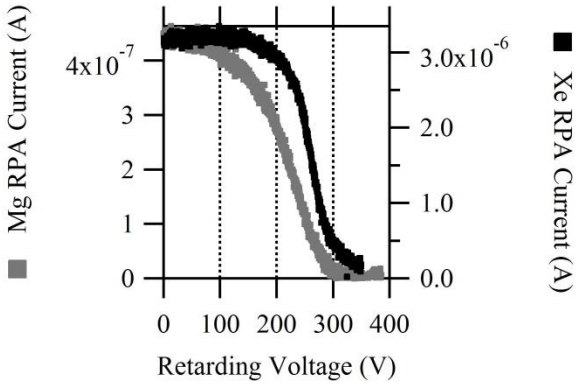

Fig. 28. Plasma current collected as a function of retarding potential. It can be clearly seen that the plasma current as a function of voltage drops more drastically at lower voltages for magnesium than for xenon propellant. For reference, the acceleration potential was held constant at 300 V for both magnesium and xenon propellant.

Assuming single ionized propellant, the ion energy distribution function (IEDF) can be obtained by taking the derivative of the current-versus-retarding-potential traces shown in Fig. 28 followed by area normalizing the derivatives. The synthetic IEDFs for magnesium ions and xenon ions are shown in Fig. 29. Comparing the IEDFs of

magnesium and xenon show conclusively that the magnesium ions are not accelerated nearly as well as the xenon ions. The most probable ion energy for magnesium propellant is ~230 V while the most probable ion energy for xenon propellant is ~260 V. To quantify the spread in ion energies, the full width at half maximum (FWHM) was measured for each IEDF. For xenon the FWHM was 55 V. For magnesium the FWHM was 107 V. The dramatic increase in the FWHM for magnesium compared to xenon indicates a much wider spread of ion energies for magnesium than xenon.

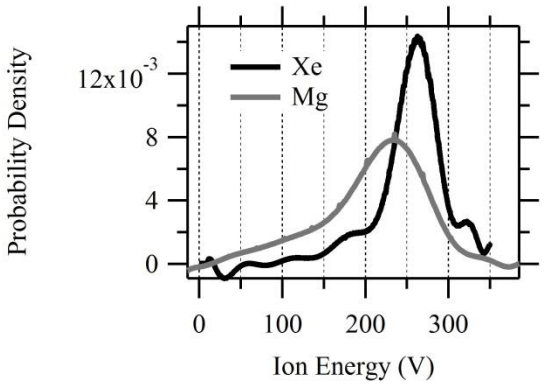

Fig. 29. Ion energy distribution function obtained by differentiating and area normalizing the current-versus-retarding-voltage traces obtained using a retarding potential analyzer in both the magnesium and xenon plasma plumes.

5.3.3. Off-axis Current Distribution

Ion current in the plasma beam was measured as a function of off-axis angle using a planar faraday probe described in detail in Section 5.2. The probe was biased to -20 V, below ion saturation, and swept in an arc centered on the face of the thruster at a radius of 250 mm. Figure 30 shows the current density in A/cm^2 as a function of off-axis angle for both the xenon plasma plume and the magnesium plasma plume. By inspection, it is clear that the xenon plasma beam is much more collimated than the magnesium plasma beam.

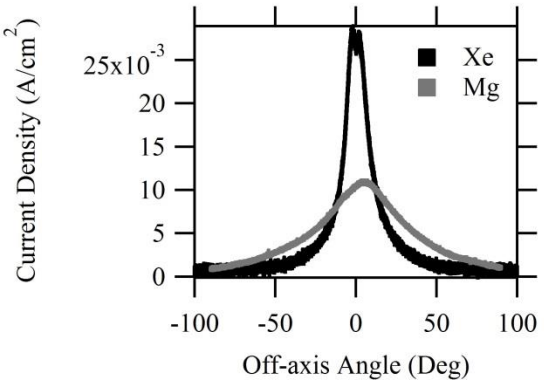

Fig. 30. The ion current density as a function of off-axis angle is shown. The current distribution for magnesium is much less collimated than the ion current distribution for xenon.

While it is clear from Fig. 30 that the xenon plasma beam is much more collimated than the magnesium plasma beam, a more quantitative comparison is shown in Fig. 31. The graph in Fig. 31 shows the percentage of beam current contained at a particular half-angle. The curves were calculated by integrating the ion current, $i(\theta)$, over a half-sphere surface and normalizing them to the total integrated ion beam current as described in equation (16), where $I_{norm}(\varphi)$ is the percentage of beam current contained in a swath from 0° (thrust axis) to φ; I_{beam} is the total integrated beam current as defined in Chapter 2.2; and $I_{beam}(\varphi)$ is the total beam current contained in a swath from 0° to φ. It is clear from Fig. 31 that higher percentages of the xenon plasma beam are contained at smaller half-angles than that of the magnesium beam, indicating more collimation for the xenon beam than the magnesium beam.

$$I_{norm}(\varphi) = \frac{I_{beam}(\varphi)}{I_{beam}} = \frac{\int_0^{\varphi} i(\theta)\sin(\theta)d\theta}{\int_0^{90} i(\theta)\sin(\theta)d\theta} \tag{16}$$

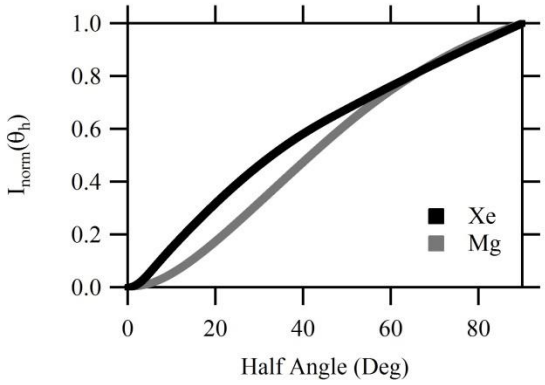

Fig. 31. Percentage of beam current contained as a function of off-axis half angle. The graph confirms that the xenon plasma beam is much more collimated than the magnesium plasma beam.

5.4. Comparing the Plume Properties of Magnesium and Xenon to Krypton and Bismuth

To fully examine the effects of changing the working gas in the thruster, two other sets of data were also used for comparison: data obtained from the plume of a BPT-2000 operated on krypton propellant from Sommerville's experiments [59] and data from the plume of a BPT-2000 operated on bismuth from Massey's experiments [15]. The data from Sommerville's experiments showed a most-probable ion energy of ~200 V using a 250 V nominal discharge voltage. Sommerville also noted a wide ion energy distribution. The data from Massey, showed a very different trend. Massey found that the most probable ion energy using bismuth was ~365 V using a nominal discharge voltage of 382 V. Both Massey and Sommerville also measured ion current density as a function of off-axis angle. Figure Fig. 32 shows the beam current fraction as a function of the off-axis angle for all four propellants and Fig. 33 shows the normalized ion collector current as a function of ion repeller voltage taken with an RPA in the plasma plume for each

propellant. For the purpose of comparison due to limited data the Faraday traces are only compared over a half angle of 47° not 90°. While there are small differences in the discharge characteristics of the thrusters operated with krypton and bismuth compared to the thrusters operated with magnesium and xenon, there was not enough difference to account for the drastic difference in plasma properties.

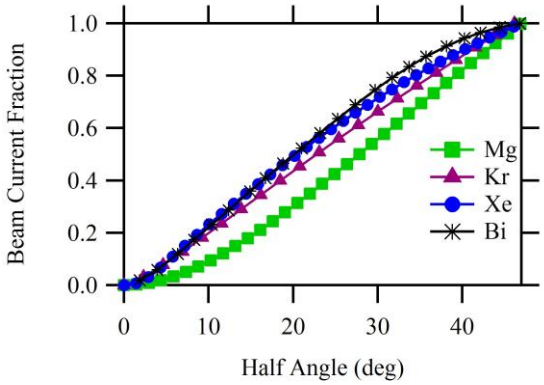

Fig. 32. Beam current fraction as a function of half angle for BPT 2000 thrusters operated using magnesium, krypton [59], xenon, and bismuth [15]. Magnesium has the most divergent beam and bismuth has the most collimated.

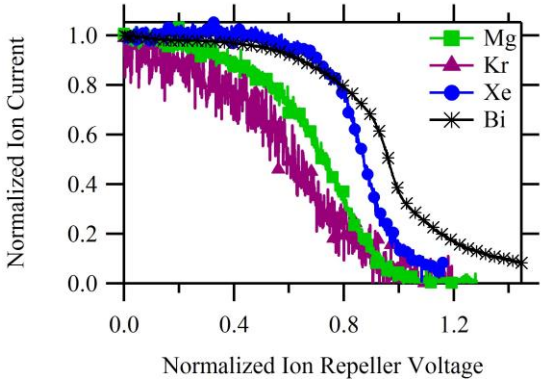

Fig. 33. Collected ion current as a function of ion repeller voltage as measured by an RPA in the plumes of BPT 2000 thrusters operated on magnesium, krypton [59], xenon, and bismuth [15]. Because the thrusters were operated at slightly different discharge conditions, the collector current was normalized to the maximum current, and repeller voltage was normalized to the discharge voltage.

5.5. Discussion

The results of the experiments show a major difference in the plasma properties of the magnesium plasma compared to the xenon plasma. The plasma properties measured by the Langmuir probe showed that the temperature and plasma potential are on the same order of magnitude for the two plasma species, but the plasma generated using magnesium gas is an order of magnitude less dense than the plasma generated using xenon gas. The most likely cause for the density decrease is a decrease in the ionization rate from xenon to magnesium. This theory is supported by the ion energy data, and ion current distribution data. The ion energy distribution function as measured by the retarding potential analyzer, described in Section 5.3.2, indicate that the ions produced using the magnesium gas are, on average, less energetic than the ions produced using the xenon gas. The reduction in ion energy in the case of magnesium is likely due to ions being born in regions of lower plasma potential—i.e. further downstream of the anode. Additionally, the magnesium plasma beam is much more divergent than the xenon plasma beam as shown by the ion current distribution data in Section 5.3.3.

The comparisons, shown graphically in Fig. 31 and Fig. 32, demonstrate that the plasma properties are heavily dependent on atomic species. Using the analysis of Brown [32], treating the thruster as a point source, the beam divergence efficiency was calculated for the plasma beams of each propellant using equation (4): beam efficiency for bismuth was 0.83, for xenon was 0.82, for krypton was 0.79, and for magnesium was 0.76. From the data it appears that the beam efficiency of the BPT 2000 is heavily dependent on propellant mass increasing by 0.07 from magnesium to bismuth. It should

be noted however that the beams of each thruster were not fully integrated; current was only collected from -47° to +47° in the case of the bismuth thruster such that integration could only take place over a half angle of 47°. However, a 47° half angle ideally encompasses the majority of the plasma beam and therefore should serve as a suitable comparison between plume structures.

The measurements made by the RPA are in good agreement with the measurements of beam divergence. Because the plasma potential was not measured at the location of the RPA for each of the measurements, the uncorrected voltage utilization was calculated using equation (5) for $V_p = 0$. The voltage utilization for bismuth was 0.96, for xenon was 0.87, for krypton was 0.80, and for magnesium was 0.77. Again the voltage utilization was higher for the heavier propellants and lower for krypton and magnesium. While the most probable ion energy for krypton as determined by Sommerville was ~200 V, the RPA signals were rather noisy and had only a minimal discernible peak in the ion energy distribution function.

Others have seen similar trends in beam divergence and ion energy and have postulated propellant utilization as the cause [32,43]. In the case of Brown's study the issues were caused by operating the thruster at low voltage [32]. In the case of studying multiple propellants, the issue is likely caused by the differences in the atomic properties of the propellants. First, the ionization potential of each working gas is different: 7.6 eV for magnesium, 14.0 eV for krypton, 12.1 eV for xenon, and 7.3 eV for bismuth. Second, if equation (10) is expanded, shown in equation (17), we see that the ionization mean free path (IMFP) depends on two atomic properties: the atomic mass of the working gas and the electron impact ionization cross-section of the working gas.

$$\lambda_i = \frac{1}{n_e \langle \sigma_i v_e \rangle} \sqrt{\frac{8 k_B T_n}{\pi M}} \tag{17}$$

Equation (17) confirms that the atomic properties of the working gas have a large effect on the ionization characteristics of the gases.

Assuming the neutral gas temperatures are on the order of the anode temperature—500 °C (793 K)—each propellant species has a different thermal velocity dependent on the atomic mass. The lighter elements would be traveling at a higher speed than the heavier elements implying they would travel farther before ionizing. There is also a significant difference in the ionization factor—the expected value of the ionization cross-section and electron energy distribution function—for each of the elements. Using the measurements from Freund and Wetzel et al. [67,68] a direct comparison of the first ionization cross section of each of the working gases can be made. Other measurements of collision cross section are available and have varying results [67-73], but the work of Freund et al. and Wetzel et al. provided ionization cross sections for each of the working gases obtained using the same measurement apparatus.

From Refs [67,68] it can be seen that the peak collision cross-section for magnesium is larger than the peak cross-section for xenon 5.3 $Å^2$ compared to 5.0 $Å^2$ shown graphically in Fig. 34. However, the ionization cross-section for magnesium peaks at a much lower temperature than the peak for xenon: 20 eV for magnesium compared to 75 eV for xenon. Moreover, the ionization cross-section for magnesium decreases rapidly with electron temperature after the peak cross-section, while the ionization cross-section for xenon remains rather flat through 100 eV. This discrepancy in the ionization cross-sections of the two propellant species is likely a large contributing factor to the

differences in the plasmas produced. The collision cross-section of krypton peaks at 3.7 $Å^2$ and is lower than the collision cross-section of xenon at all electron temperatures from 0-200 eV. The collision cross-section of bismuth peaks at 8.8 $Å^2$ and is much greater than xenon's collision cross-sections at each electron temperature from 0-200 eV.

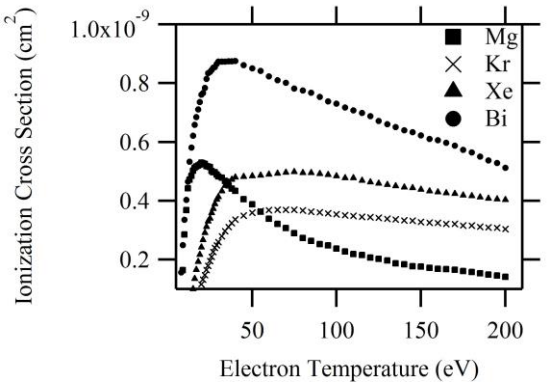

Fig. 34. Absolute collision cross-section for electron impact ionization (single) [67,68].

Using equation (17), the ionization mean free path was calculated for each propellant for an electron density of 1 x 10^{18} m^{-3} and a neutral temperature of 500 °C (793 K) as a function of Maxwellian electron temperature from 10 eV to 100 eV, shown in Fig. 35. Subsequently the ratio of IMFP of each propellant to xenon was calculated verses electron temperature and is plotted in Fig. 36.

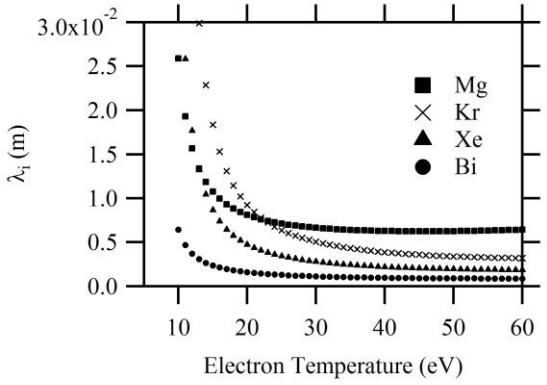

Fig. 35. Ionization mean free path as a function of electron temperature for magnesium, krypton, xenon, and bismuth. Electron density was assumed to be 1 x 10^{18} m^{-3} and a neutral temperature of 793 K was used.

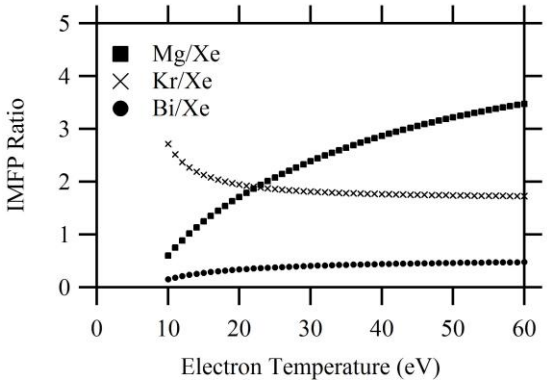

Fig. 36. The calculated ratio of magnesium ionization mean free path to xenon ionization mean free path as a function of electron temperature using a neutral temperature of 793 K.

Looking at Fig. 35 and Fig. 36, it can be seen that at increased electron temperatures the ionization mean free paths of krypton and magnesium are significantly longer than that of xenon. Magnesium and krypton may be penetrating into the acceleration regions upwards of 2-4 times further than xenon, causing the observed differences in plume properties. This would indicate that lengthening the discharge channel would be a logical solution to improving the beam properties. But, in addition to the ionization mean free path, the propellant utilization efficiency also depends on the number of ions lost to the discharge chamber walls. Cohen-Zur et al. performed a study in which theoretical analysis of propellant utilization was investigated [62]. In their study, Cohen-Zur et al. solved the fluid continuity equations at the exit plane of the thruster in order to approximate propellant utilization as a function of the ionization mean free path, λ_i, and the mean free path for ion loss to the channel wall, λ_w. The result of their work is shown in equation (18).

$$\eta_p = \frac{1}{1-\lambda_i/\lambda_w}\left[1-\exp\left(-\frac{L_c}{\lambda_i}\left[1+\frac{\lambda_i}{\lambda_w}\right]\right)\right] \tag{18}$$

In equation (18), the wall loss is determined by equation (19) where h^2 is the channel height, L_c is the channel length, and V_d is the discharge voltage.

$$\lambda_w = \frac{eV_d h^2}{2T_e L_c} \tag{19}$$

Essentially equation (18) implies that the propellant utilization for a certain working gas depends on the discharge voltage (electron temperature), the length of the channel, and the mass flow rate of the thruster. Therefore, in the case of a matched molar flow rate and discharge voltage—as with the comparison of magnesium and xenon in Section 5.3—the only way to improve the propellant utilization would be to lengthen the channel. Using equation (19) propellant utilization was calculated as a function of normalized channel length, for an electron density of 1 x 10^{18} m^{-3}, a discharge voltage of 300 V, an electron temperature of 30 eV, and a neutral temperature of 793 K.

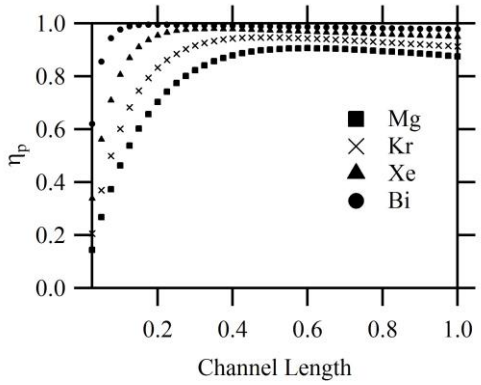

Fig. 37. Propellant utilization as a function of normalized channel length for a discharge voltage of 300 V, an electron temperature of 30 eV, and an electron density (proportional to mass flow rate) of 1 x 10^{18} m^{-3}. The peak propellant utilization efficiency for magnesium propellant occurs with a longer channel than that of each of the other propellants.

As can be seen in Fig. 37 it is clear that the propellant utilization of magnesium-fueled thruster is a likely culprit for the properties of the plasma beam and the decreased

thruster efficiency seen in Chapter 4. While lengthening the thruster channel appears to increase the propellant utilization to a point, eventually the increased wall losses dominate over the increased ionization. The solution to the problem will be to using modern magnetic field designs to deflect the ions ionized early in the discharge chamber toward the chamber centerline and minimize wall losses. It has been shown in simulation [74] and experiment [75] that shaping the magnetic field to run parallel with the discharge chamber walls shapes the potential profile inside the discharge chamber such that ions are focused away from the walls towards the chamber centerline. The original intent of the technology was to mitigate wall erosion, but the same technology should increase the operation efficiency of thrusters using propellants other than xenon by enabling longer discharge channels with minimal ion losses to the walls.

5.6. Conclusion

A direct comparison of plasma properties was made between a Hall-effect thruster operating on magnesium propellant to xenon propellant. Measurements of plasma properties using a double Langmuir probe—electron temperature, plasma density, and plasma potential—revealed a large difference in plasma densities: the magnesium plasma was much less dense at the same propellant flow rate. Measurements of ion energy using a retarding potential analyzer revealed that the magnesium ions had significantly less energy. Current density measured downstream from the thruster as a function of off-axis angle showed that the magnesium plasma beam was much more divergent than the xenon plasma beam.

Analysis of the atomic properties of magnesium, krypton, xenon, and bismuth coupled with comparisons of plasma properties of all four propellants indicate that the atomic properties of the working gas play a major role in the plasma generation of the thruster and likely the efficiency. Analysis of the calculated mean free path for ionization of each of the four propellants indicates that magnesium and krypton require much longer distances for ionization than xenon and bismuth. This discrepancy in the distance required for ionization explains the differences in beam and voltage utilization efficiencies—lower atomic mass was correlated with decreased efficiency. If the magnesium atoms travel longer distances before an ionization event then the generated plasma is likely to have reduced ion energy, larger beam divergence, and lower overall densities.

In general this study shows that alternative propellants cannot be substituted one-for-one in any Hall thruster. Rather a thruster must be designed for a particular propellant. In order to correct the discrepancies, physical modifications should be made to Hall thrusters using different propellants—particularly light propellants. A longer and thinner channel would enact multiple benefits. A longer channel has been shown to collimate the plasma beam and as well as increase ionization efficiency [63] though any lengthening of the channel must be balanced with the increased ion losses to the wall [62]. Lowering the electron temperature could be achieved by reducing the channel width which may increase ionization rates for the magnesium plasma [61] but needs to be balanced by the increased wall losses due to interception of ions. Reducing the discharge voltage would also lower the electron temperature, and in some cases may be desirable as in direct drive missions. Finally, using the magnetic field design of Mikellides et al. [74] and Hofer et

al. [75] the issue of propellant utilization could be eliminated by eliminating wall losses in Hall thrusters with lengthened discharge channels.

Chapter 6

Conclusions/Direction of Future Work

The goal of this work was to evaluate magnesium as a Hall thruster propellant. At the start of the project, there was no method of operating the thruster for long periods of time at mission-relevant voltages, nor was there a way to operate the thruster with the power supplies in voltage-limited mode. While studies had been performed using magnesium as a propellant, none had measured the performance of a thruster using magnesium propellant, nor had there been measurements of the plasma properties in the thruster plume.

6.1. Thermal Mass Flow Control

In designing the thermal mass flow control system, the state-of-the-art methods of operating condensable propellant Hall thrusters were evaluated. Two distinct methods had been used in literature: (1) external propellant reservoirs and external evaporators supplied propellant to the thruster via heated propellant lines and (2) a reservoir internal to the thruster such that the waste heat from the thruster discharge supplied all of the heat necessary for propellant evaporation.

The benefits of both methods—precise control of method (1) and high efficiency of method (2)—were combined to create the thermal mass flow control system. Waste heat

from the thruster discharge drives the majority of the evaporation while a supplemental heater provides fine-tuned control of the evaporation rate. The control window was achieved by reducing the open area of the anode such that the power deposited on the anode from the plasma discharge was not suitable to drive enough evaporation for sustained thruster operation; some additional power was needed. This system allowed for thruster operation for long duration, on the order of hours, at high efficiency—only a 6% decrease due to thermal power for the heater. The system also allows for precise control of the discharge current and therefor the mass flow rate. Appendix B demonstrates the scalability of the thermal mass flow control system.

6.2. Performance of the BPT 2000 using Magnesium Propellant

One of the main evaluation points of magnesium as a Hall thruster propellant is its performance as measured by thrust, specific impulse, and efficiency. For most thrusters, the measurement of performance is as simple as placing the thruster on a thrust stand and measuring thrust as a function of mass flow rate and discharge voltage. However, the magnesium thruster presents some unusual issues. First, the thruster is ignited after a heating cycle, which causes thermal drift issues with the thrust stand. Additionally and more importantly, there is no way to measure the mass flow rate of magnesium in situ.

To solve the problem of measuring mass flow rate in the magnesium thruster, a time-averaged method of measuring the mass flow rate was developed. In this method the mass flow rate was determined by measuring the total mass lost during thruster operation and the mass lost during heating of the thruster, cooling of the thruster, and the transition

period between initial ignition and stabilization. Subtracting the mass lost during heating, cooling, and transition from the total mass lost gives the mass used during stable thruster operation. Dividing the mass lost during stable operation by the amount of time the thruster was stable gives an accurate measurement of mass flow rate.

Using the corrected, time-averaged mass flow rate performance was measured at 4 operating conditions: 300 V at 7 A, 300 V at 5 A, 250 V at 7 A, and 200 V at 7 A. The performance results indicated that magnesium enables very high specific impulses as expected—on the order of 2500 s at 300 V discharge. The efficiency of the thruster, however, was very low—on the order of 24%. This efficiency is very low even with a baseline efficiency of 40% using xenon propellant in the same thruster. In order for magnesium to be a useful propellant a large improvement in efficiency must be achieved.

6.3. Properties of the Magnesium Plasma Plume and Implications on Thruster Design

In order to better understand the operation of the magnesium-fueled thruster, to propose reasons for the low performance, and to propose methods to improve the performance, measurements of the plasma properties in the plume of the magnesium thruster were compared to plasma measurements take in the plumes of krypton-, xenon-, and bismuth-fueled thrusters of the same model: the BPT 2000.

A direct comparison of plasma properties measured in the magnesium plume were compared to plasma properties measured in a xenon plume at analogous operating conditions: 300 V at 5 A of discharge current. The results showed that the magnesium beam is much more divergent than the xenon beam; the plasma density in the magnesium

beam is much lower than the xenon beam (on-axis); and the ion energy in the magnesium beam is lower than in the xenon beam on average. When the properties of several propellants are compared—magnesium, krypton, xenon, and bismuth—there is a distinct pattern: the lower the ionization mean free path the more collimated the plasma beam and the higher the ion energy. The longer ionization mean free paths of magnesium and krypton correlate well to the lower performance of the propellants. From these results, it is apparent that physical modifications to the thruster would be needed to improve performance of magnesium (and krypton).

The main implication of the plume properties is that magnesium cannot be substituted for xenon in pre-existing Hall thrusters. Analysis showed that increasing the length of the discharge channel could increase the propellant utilization efficiency, but the increases would eventually be overwhelmed by increased wall losses. A thruster designed for magnesium would need to use magnetic shielding to limit ion losses to the walls.

6.4. Overall Conclusions and Future Work

After creating a method for operating the magnesium thruster stably for long-durations, measuring the performance of the magnesium thruster, and measuring the properties of the plasma plume, it is clear that there are some major difficulties with magnesium propellant. The efficiency of the thruster using magnesium propellant is 43% lower than the efficiency of the xenon thruster, the plasma plume is much more divergent, and the ion energy is much lower. However these detriments are not completely unexpected since the thruster was designed for operation using xenon. Considering the ionization mean free path calculated in Chapter 5 Subsection 5.4, it is

clear that (1) the thruster would need to use magnetic shielding (2) the discharge chamber should be substantially lengthened. The improved efficiency from a thruster redesign may improve the overall efficiency of a magnesium-fueled thruster. The redesign coupled with the low-voltage peak in magnesium ionization cross section may mean that low-voltage, direct-drive missions that require high Isp are a good niche for magnesium. Using magnesium propellant, moderate to high specific impulses (1500 s – 2000 s) may be achievable at voltages as low as 100 V if thruster efficiency is improved.

Given the issues of operating a Hall thruster designed for xenon propellant, using magnesium propellant, the most obvious future work is to design a thruster specifically for magnesium propellant. Assuming the technology is proven, replication of the technology can be performed and parallel efforts can occur at multiple academic institutions without prohibitive capital investments in high-capacity vacuum pumps. Once a working, high-efficiency magnesium thruster is designed, it could enable high-power, high-Isp, low-voltage direct drive missions for travel to and from Mars with the possibility of in-situ resource utilization as desired by HEFT. A high efficiency magnesium thruster would also enable high-Isp multi-target main belt missions at a much lower cost than using ion engines.

Appendix A. Facility Pressure during Magnesium Thruster Operation

While the advantages of condensable propellants may enable certain Hall thruster missions that would not be possible with xenon, one of the biggest benefits is realized during thruster development. The trend in Hall thruster development is currently moving towards higher and higher powers (upwards of 100 kW). Very few facilities are capable of testing these new thrusters operating at such high powers using xenon propellant, and few, if any university-scale facilities are suitable (see Chapter 2.1). However, condensable propellants—bismuth, zinc, and magnesium, in particular—are solid at room temperature and will condense on the walls of the vacuum facility, eliminating the need for high capacity cryogenic pumps. Because the entire inner surface of the vacuum facility acts like a cryogenic surface, condensable propellants should in principle enable high power Hall thruster testing in university-scale facilities. Unfortunately measuring the partial pressure of an ionized metal vapor at very low pressures (~10^{-5} torr) is not possible with conventional pressure measurement devices and so the ground testing benefits of condensable propellants has not yet been verified.

There are many devices available for measuring pressure in high vacuum. Some of the most common devices are hot cathode ionization gauges, cold cathode ionization gauges, and capacitance monometers. Unfortunately, none of these devices are suitable for

measuring the pressure of a metallic vapor. The conductive coatings that form on the device tend to skew measurements or even irreparably damage the instrument. For this reason, the pressure of the metal vapor will be measured using non-traditional methods: a quartz crystal microbalance (QCM) will be used to measure the condensation rate of metal in time from which the pressure can be determined. The following analytic investigation will demonstrate the feasibility of using a QCM to determine pressure and layout the necessary experimental framework.

Assuming an equilibrium ideal gas, the number of gas particles incident on a surface is given by equation (20) [76] where N is the number of particles, t is time, S is the surface area, P is pressure, k_B is the Boltzmann constant, T is temperature, M is the mass of the gas particle, and v is the velocity of the gas particle perpendicular to the surface.

$$\frac{d^3N}{dtdS} = \frac{P}{k_BT}\int_0^\infty \sqrt{\frac{M}{2\pi k_BT}}\exp\left(\frac{-Mv^2}{2k_BT}\right)vdv = \frac{P}{M}\sqrt{\frac{M}{2\pi k_BT}} \tag{20}$$

To determine the mass accumulation rate on a surface the ratio of the number of incident atoms that condense on the surface to the total number of incident atoms on the surface—the sticking coefficient, η_s—must be taken into account. For a sticking coefficient less than unity, the rate at which mass, m, will accumulate is predicted by equation (21).

$$\frac{d^3m}{dtdS} = \eta_s P\sqrt{\frac{M}{2\pi k_BT}} \tag{21}$$

The graph in Fig. 38 shows equation (21) plotted over three decades of pressure. The sticking coefficient used was that which was found by Zhou et al [77]. Zhou et al

measured the sticking coefficient of magnesium incident on aluminum oxide as a function of the substrate temperature and as a function of the thickness of the accumulated magnesium. For the experiments reported here magnesium was incident on a substrate already coated in magnesium at temperatures less than 50°C; for such conditions the sticking coefficient was found to be 0.30 [77].

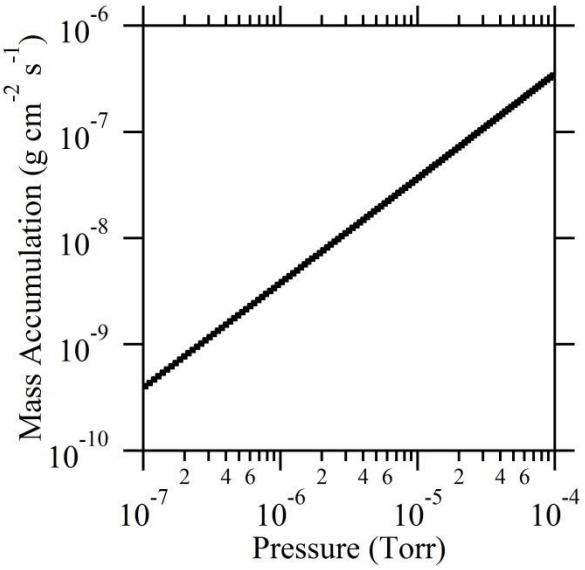

Fig. 38. A graph of depicting the rate at which mass will accumulate on a surface when exposed to condensable magnesium vapor at a given pressure for a sticking coefficient of 0.30.

The goal of this research was to measure the partial pressure of residual magnesium vapor during operation of magnesium-fueled Hall thrusters. Pressure measurements were obtained during operation of a 2 kW thruster.

The experiments took place in the CPF with an ultimate base pressure of 10^{-6} torr measured by a Bayard-Alpert hot cathode ionization gauge. The thruster used in the experiments was a laboratory thruster based on the Aerojet BPT-2000 Hall thruster. Mass accumulation measurements were made using an Inficon SQM-160 with a front load, single sensor, water-cooled crystal. Because the correlation of mass accumulation rate to

pressure requires the assumption of a Maxwellian gas, the crystal must be intelligently located. There are no locations downstream of the thruster where the gas is Maxwellian, so the crystal was placed on the thrust axis behind the thruster. Magnesium vapor behind the thruster is the result of expelled propellant colliding with surfaces downstream of the thruster until migrating back behind the thruster; for this reason the gas can be assumed to be mostly Maxwellian. Additionally locating the QCM behind the thruster shielded the QCM from direct, high-energy beam flux. The experimental setup is shown schematically in Fig. 39.

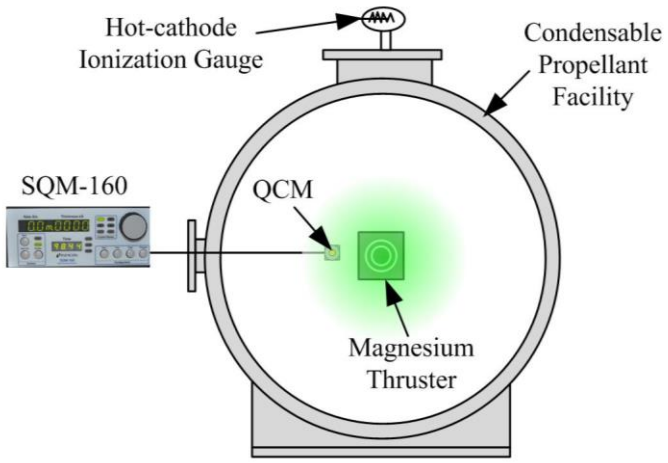

Fig. 39. Schematic of experimental setup. The position of the QCM is exaggerated for clarity. During experiments the QCM will be located on the thrust axis behind the thruster.

Measurements of mass accumulation were correlated to pressure for thruster discharges at 200 V 7 A, 250 V 7 A, 300 V 7 A, and 300 V 5 A. The error bars of pressure were calculated using sticking coefficients of 1 and 0.03 representing the extreme conditions of each atom hitting and sticking on the first wall collision and almost none of the atoms hitting and sticking on the first wall collision. The results of a typical experiment are shown in Fig. 40. As one would expect, the time at which the mass

accumulation curve begins to rise (at the7 min mark) is the same time where discharge current is initiated on the thruster.

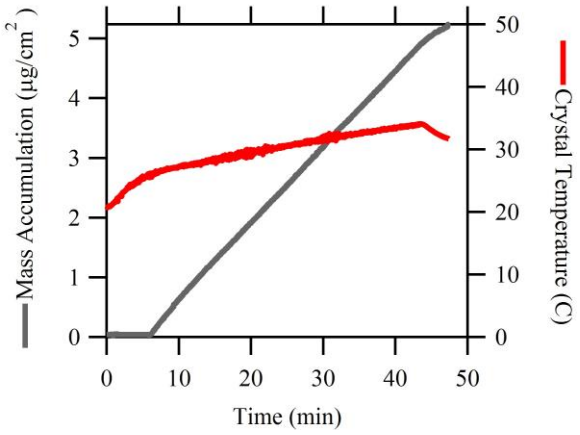

Fig. 40. Raw mass accumulation data accompanied by measurements of crystal temperature as obtained by a thermal couple attached to the QCM crystal holder.

The processed data from the experiments are shown in Fig. 41. As seen from the graph the calculated partial magnesium pressures average to 5.0 x 10^{-7} Torr, well below the normal background pressures of Hall thrusters operating using xenon propellant. Moreover, the worst-case pressures—calculated with 0.03 sticking coefficient—were still well below 10^{-5} Torr.

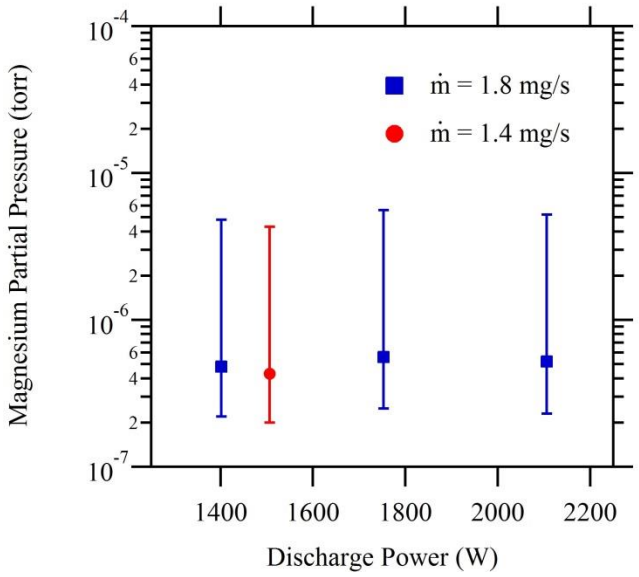

Fig. 41. The pressure calculated from mass accumulation measurements made using a QCM versus discharge power. The sticking coefficient used was 0.3 from Zhou et al. and the error bars were calculated using sticking coefficients of 1 and 0.03.

The results of the experiments showed that is possible to perform low-pressure testing of a 2-kW magnesium-fueled Hall thruster without using high-capacity cryogenic vacuum pumps. Unfortunately, because the sticking coefficient of magnesium is difficult to determine and there was no way to calibrate the QCM measurements, the measurements of pressure are highly uncertain and need to be verified in future experiments.

Appendix B. Modifying a 5 kW Thruster for Operation using Magnesium

As mentioned in Chapter 2, the current trend in Hall thruster development is toward higher and higher thruster powers approaching and exceeding hundreds of kilowatts. Therefore one of the important metrics with which to evaluate magnesium as a propellant is the ability of the technology to scale up to higher powers. In order to demonstrate scalability a UM-AFRL P5 was modified to operate using magnesium propellant.

First, in order to operate the P5 on magnesium using the thermal mass flow control system an anode must be constructed. The most critical parameter for the anode is the ratio of open area to the cross-sectional surface area of the anode. From Book and Walker [78], we know the temperature at which the P5 anode face normally operates: ~410° C at 300 V and 5 mg/s Xe and ~490 V at 300 V 10 mg/s Xe. Because it is the temperature of the anode face that drives the evaporation of the stored propellant, the open area of the anode face was chosen to ensure that the desired flow rate occurs at a temperature slightly higher than that achieved with only plasma attachment. The open area of anode used in the magnesium-fueled BPT-2000 is 1.48×10^{-5} m^2 and the total area of the anode face is 4.81×10^{-3} m^2. The total area of the P5 anode face is 8.80×10^{-3} m^2, nearly twice the surface area of the BPT-2000 anode. Because the surface area of the face of the P5 anode is approximately twice that of the BPT 2000 anode face, the initial chosen open

area of the P5 magnesium anode was chose to be twice the open area of the BPT 2000 anode. As a check on the chosen open area, the mass flow rate of the magnesium through the P5 anode open area was calculated as a function of anode temperature using equation (8) and the vapor pressure of magnesium found in the Handbook of Chemistry and Physics [79]. Figure 42 shows the mass flow rate as a function of temperature for an open area of 2.97 x 10^{-5} m^2. Two magnesium mass flow rates are highlighted in the figure: 0.922 mg/s and 1.846 mg/s. These mass flow rates are the molar-flow equivalent of 5 mg/s of Xe and 10 mg/s of Xe respectively. Both flow rates occurred at higher temperatures than achieved during normal operation of the P5, allowing for thermal mass flow control using a supplemental heater as described in Chapter 3.

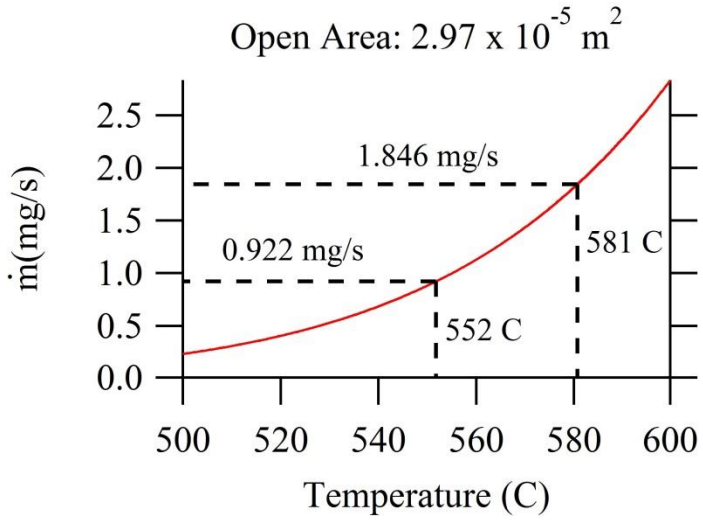

Fig. 42. Mass flow rate versus temperature for an anode open area of 2.97 x 10^{-5} m^2. The two highlighted mass flow rates are analogous to the xenon flow rates used by Book and Walker [78].

Using the analytic calculation of mass flow rate shown in Fig. 42, an anode was constructed for the P5, which was hollow, to hold solid magnesium propellant and had an open area of 2.97 x 10^{-5} m^2. The second necessary component for implementing the

thermal mass flow control system with the P5 was to create a supplemental anode heater. As with the BPT-2000 supplemental heater, a resistive heater was constructed with counter wound coils to eliminate parasitic axial magnetic field. The heater element was constructed of 0.02-inch thick graphite paper sandwiched between boron nitride plates to isolate the heater from anode potential. A quarter-section view of the modified P5 Hall thruster is shown in Fig. 43.

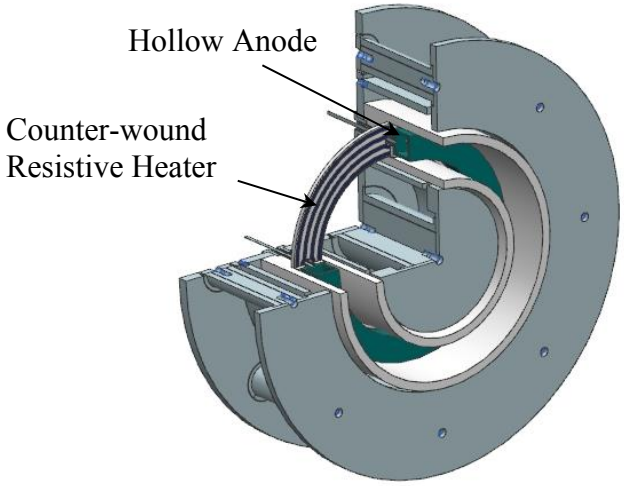

Fig. 43. Cutaway of a UM-AFRL P5 Hall thruster modified for use with magnesium. Highlighted are the counter-wound resistive supplemental heater and the hollow anode used for propellant storage, gas distribution, and ion acceleration.

Once the P5 anode and heater were fabricated, the anode was loaded with propellant and the thruster was assembled. Then the thruster was installed in the Condensable propellant facility. Using the same methods outlined in Chapter 4, the P5 was heated and ignited. Figure 44 shows images of the P5 before and during operation. In an unprecedented turn of events, the thruster was ignited on the first try, using the first fabricated heater and anode. While sometimes aberrations occur in nature, such as the lighting of the thruster on the first try, such aberrations are always corrected. After

several minutes of operation a second plasma discharge occurred on the P5 mostly composed of stainless steel and Kapton tape, the results are shown in Fig. 45. After repairing the melted anode support the P5 was once again ignited. The results of the experiment are shown in Fig. 46. While the P5 never achieved steady-state constant-voltage operation, it did remain lit for more than an hour. Future studies attempting different magnetic coil currents would likely enable constant-voltage operation.

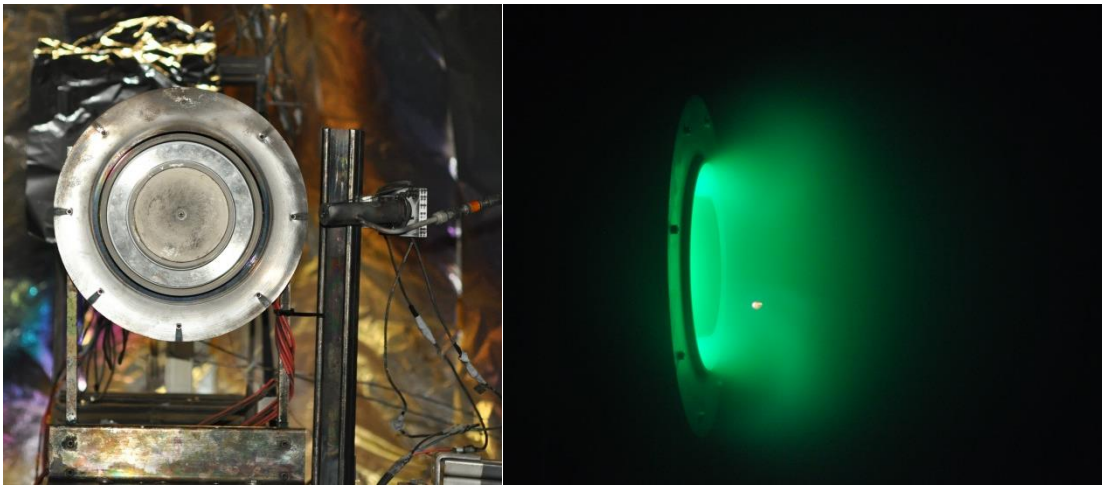

Fig. 44. LEFT: The P5 modified for operation with magnesium propellant mounted in the Condensable Propellant Facility. RIGHT: The P5 operating on magnesium propellant.

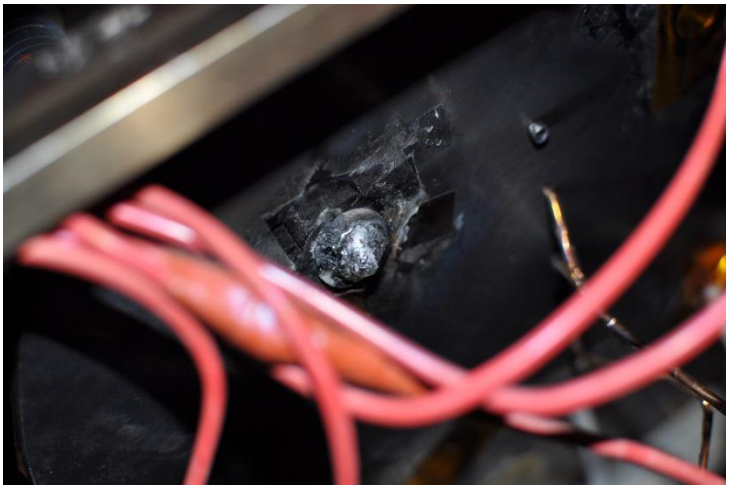

Fig. 45. The results of plasma attaching to an anode support on the backside of the P5—a mildly deformed 6-32 nut and bolt.

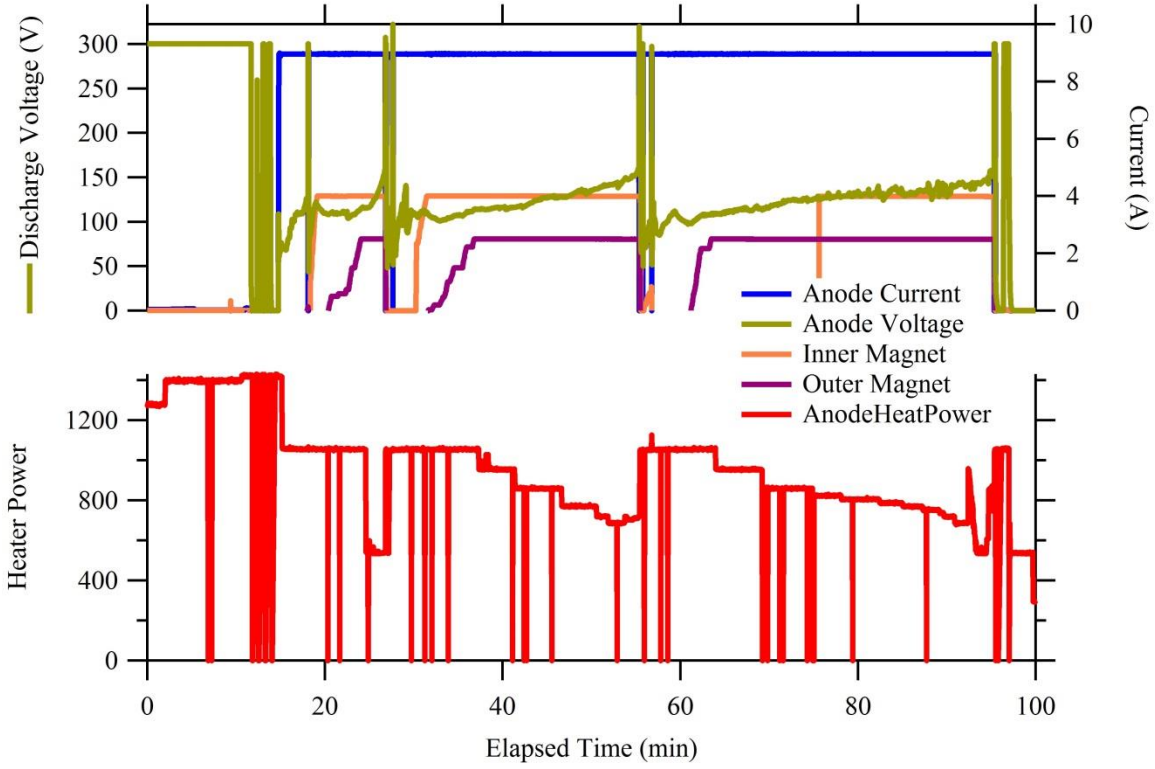

Fig. 46. Telemetry of a P5 thruster test beginning shortly before thruster ignition. Unfortunately, constant-voltage operation was not achieved but is likely due to excessive magnetic field strengths.

References

[1] Choueiri, E.Y., "Plasma oscillations in Hall thrusters," Physics of Plasmas, 8, 2001, pp. 1411-1426

[2] Kim, V., "Main Physical Features and Processes Determining the Performance of Stationary Plasma Thrusters," Journal of Propulsion and Power, 14, 1998, pp. 736-743

[3] King, L.B. and A.D. Gallimore, "Ion-Energy Diagnostics in an SPT-100 Plume from Thrust Axis to Backflow," Journal of Propulsion and Power, 20, 2004, pp. 228-242

[4] Hofer, R.R., "Development and Characterization of High-Efficiency, High-Specific Impulse Xenon Hall Thrusters," *Doctoral Dissertaion*, Aerospace Engineering, University of Michigan, 2004

[5] Hofer, R.R., R.S. Jankovsky, and A.D. Gallimore, "High-Specific Impulse Hall Thrusters, Part 1: Influence of Current Density and Magnetic Field," Journal of Propulsion and Power, 22, 2006, pp. 721-731

[6] Hofer, R.R. and A.D. Gallimore, "High-Specific Impulse Hall Thrusters, Part 2: Efficiency Analysis," Journal of Propulsion and Power, 22, 2006, pp. 732-740

[7] Gnedenko, V.G., V.A. Petrosov, and A.V. Trofimov, "Prospects for Using Metals as Propellants in Stationary Plasma Engines of Hall-Type," *23rd Internation Electric Propulsion Conference,* IEPC-1995-54, Moscow, Russia, 1995

[8] Szabo, J., B. Pote, S. Paintal, M. Robin, G. Kolencik, A. Hillier, R.D. Branam, and R.E. Huffman, "Performance Evaluation of an Iodine Vapor Hall Thruster," *47th AIAA/ASME/SAE/ASEE Joint Propulsion Conference & Exhibit,* AIAA 2011-5891, San Diego, CA, 31 July - 03 August

[9] Landis, G.A., "Materials Refining on the Moon," Acta Astronautica, 60, 2007, pp. 906-915

[10] Banin, A. and R.L. Mancinelli, "Life on Mars? I. The Chemical Environment," Adv. Space Res., 15, 1995, pp. 163-167

[11] Tverdokhlebov, S.O., A.V. Semenkin, and J.E. Polk, "Bismuth Propellant Option for Very High Power TAL Thruster," *40th AIAA Aerospace Sciences Meeting & Exhibit,* AIAA-2002-0348, Reno, NV, 14-17 January 2002

[12] Marrese-Reading, C., A. Sengupta, R. Frisbee, J.E. Polk, M. Cappelli, I. Boyd, M. Keidar, S.O. Tverdokhlebov, A.V. Semenkin, T. Markusic, A. Yalin, and T. Knowles, "The VHITAL Program to Demonstrate the Performance and Lifetime of a Bismuth-Fueled Very High Isp Hall Thruster," *41st AIAA/ASME/SAE/ASEE Joint Propulsion Conference & Exhibit,* AIAA-2005-4564, Tucson, AZ, 10-13 July 2005

[13] Makela, J.M., D.R. Massey, and L.B. King, "Bismuth Hollow Cathode for Hall Thrusters," Journal of Propulsion and Power, 24, 1, 2008, pp. 142-146

[14] Makela, J.M., D.R. Massey, L.B. King, and E.C. Fossum, "Development and Testing of a Prototype Bismuth Cathode for Hall Thrusters," *41st AIAA/ASME/SAE/ASEE Joint Propulsion Conference & Exhibit,* AIAA-2005-4236, Tucson, AZ, 10-13 July 2005

[15] Massey, D.R., "Development of a Direct Evaporation Bismuth Hall Thruster," *Doctoral Dissertation*, Mechanical Engineering-Engineering Mechanics, Michigan Technological University, 2008

[16] Massey, D.R., A.W. Kieckhafer, J.D. Sommerville, and L.B. King, "Development of a Vaporizing Liquid Bismuth Anode for Hall Thrusters," *40th AIAA/ASME/SAE/ASEE Joint Propulsion Conference & Exhibit,* AIAA-2004-3768, Fort Lauderdale, FL, 12-14 July 2004

[17] Massey, D.R., L.B. King, and J.M. Makela, "Progress on the Development of a Direct Evaporation Bismuth Hall Thruster," *29th International Electric Propulsion Conference,* IEPC-2005-256, Princeton, NJ, 31 October - 4 November 2005

[18] Hopkins, M.A. and L.B. King, "Performance Characteristics of a Magnesium Hall Thruster," *32nd International Electric Propulsion Conference*, IEPC-2011-299, Wiesbaden, Germany, 11-15 September 2011

[19] Hopkins, M.A., J.M. Makela, R.L. Washeleski, and L.B. King, "Mass Flow Control in a Magnesium Hall-effect Thruster," *45th AIAA/ASME/SAE/ASEE Joint Propulsion Conference & Exhibit,* AIAA-2010-6861, Nashville, TN, 25-28 July 2010

[20] Makela, J.M., R.L. Washeleski, L.B. King, D.R. Massey, and M.A. Hopkins, "Development of a Magnesium and Zinc Hall-effect Thruster," Journal of Propulsion and Power, 26, 2010, pp. 1029-1035

[21] Szabo, J., M. Robin, and J. Duggan, "Light Metal Propellant Hall Thrusters," *31st International Electric Propulsion Conference,* IEPC-2009-138, Ann Arbor, MI, 20-24 September 2009

[22] Szabo, J., M. Robin, S. Paintal, B. Pote, and V. Hruby, "High Density Hall Thruster Propellant Investigations," *48th AIAA/ASME/SAE/ASEE Joint Propulsion Conference & Exhibit,* AIAA-2012-3853, Atlanta, GA, 30 July - 1 August 2012

[23] Dankanich, J.W., "Electric Propulsion for Small Body Missions," *46th AIAA/ASME/SAE/ASEE Joint Propulsion Conference & Exhibit,* Mg Mission, Nashville, TN, 25 - 28 July 2010

[24] Kamhawi, H., T.W. Haag, W. Hueng, R. Shastry, L.R. Pinero, T. Peterson, J.W. Dankanich, and A. Mathers, "High Voltage Hall Accelerator Propulsion System Development for NASA Science Missions," *Aerospace Conference 2013, IEEE,* Big Sky, MT, 2-9 March 2013

[25] Oh, D.Y., "Evaluation of solar Electric Propulsion Technologies for Discovery-Class Missions," Journal of Spacecraft and Rockets, 44, 2007, pp. 399-411

[26] Herman, D.A., G.C. Soulas, and M.J. Patterson, "Performance Evaluation of the Prototype Model NEXT Ion Thruster," *43rd AIAA/ASME/SAE/ASEE Joint Propulsion & Exhibit,* Cincinnati, OH, 8-11 July 2007

[27] *HEFT Phase 1 Closeout*, 2010, NASA.

[28] Stoker, C.R., J.L. Gooding, T. Roush, A. Banin, D. Burt, B.C. Clark, G. Flynn, and O. Gwynne, "The physical and chemical properties and resource potential of Martian surface soils", in *Resources of near-earth space*,1993, p. 659-707.

[29] Hoffman, D.J., T.W. Kerslake, J.S. Hojnicki, D.H. Manzella, R.D. Falck, H.A. Cikanek III, M.D. Klem, and J.M. Free, "Concept Design of High Power Solar Electric Propulsion Vehicles for Human Exploration," *62nd International Astronautical Congress,* Cape Town, South Africa, 3-7 October, 2011

[30] Hofer, R.R. and T.M. Randolph, "Mass and Cost Model for Selecting Thruster Size in Electric Propulsion Systems," Journal of Propulsion and Power, 29, 2013, pp. 166-177

[31] Capadona, L.A., J.M. Woytach, T.W. Kerslake, D.H. Manzella, R.J. Christie, T.A. Hickman, R.J. Scheidegger, D.J. Hoffman, and M.D. Klem, "Feasibility of Large High-Powered Solar Electric Propulsion Vehicles: Issues and Solutions," *AIAA Space 2011 Conference & Exposition,* AIAA 2011-7251, Long Beach, CA, 27-29 September, 2011

[32] Brown, D.L., "Investigation of Low Discharge Voltage Hall Thruster Characteristics and Evaluation of Loss Mechanisms," *Doctoral Dissertation*, Aerospace Engineering, The University of Michigan, 2009

[33] *INFINIUM™ Fueled Anodes for Primary Metal Production*, IFINIUM, 2013.

[34] Kramer, D.A., *2011 Minerals Yearbook, Magnesium [Advance Release]*, USGS, 2012.

[35] Meyer, M., L. Johnson, B. Palaszewski, D.M. Goebel, H. White, and D. Coote, *In-Space Propulsion Systems Roadmap*, NASA, 2012.

[36] Dankanich, J.W., M.W. Swiatek, and J.T. Yim, "A Step Towards Electric Propulsion Testing Standards: Pressure Measurements and Effective Pumping Speeds," *48th AIAA/ASME/SAE/ASEE Joint Propulsion Conference,* Atlanta, GA, 29 Jul. - 01 Aug. 2012

[37] Espe, W., M. Knoll, and M.P. Wilder, "Getter Materials for Electron Tubes," Electronics, 23, 1950, pp. 80-86

[38] Wagener, S., "A Method for Measuring the Efficiency of Getters at Low Pressures," Brittish Journal of Applied Physics, 1, 1950, pp. 225-231

[39] Goebel, D.M. and I. Katz, *Fundamentals of electric propulsion: ion and Hall thrusters*. Vol. 1. 2008: Wiley.

[40] Linnel, J.A. and A.D. Gallimore, "Internal plasma measurements of a Hall thruster using plasma lens focusing," Physics of Plasmas, 13, 103504 (2006);

[41] Linnel, J.A. and A.D. Gallimore, "Efficiency Analysis of a Hall Thruster Operating with Krpton and Xenon," Journal of Propulsion and Power, 22, 2006, pp. 1402-1412

[42] Linnel, J.A., "An Evaluation of Krypton Propellant in Hall Thrusters," *Doctoral Dissertation*, Aerospace Engineering, University of Michigan, 2007

[43] Linnel, J.A. and A.D. Gallimore, "Internal plasma potential measurements of a Hall thruster using xenon and krypton propellant," Physics of Plasmas, 13, 093502 (2006); doi: 10.1063/1.2335820

[44] Sankovic, J.M., J.A. Hamley, and T.W. Haag, "Performance Evaluation of the Russian SPT-100 Thruster at NASA LeRC," *23rd International Electric Propulsion Conference,* IEPC-93-94, Seattle, WA, September 1993

[45] Randolph, T., V. Kim, K. Kozubsky, V. Zhurin, and M. Day, "Facility Effects on Stationary Plasma Thruster Testing," *23rd International Electric Propulsion Conference*, IEPC-93-93, Seatle, WA, September 1993

[46] Hofer, R.R., P.Y. Peterson, and A.D. Gallimore, "Characterizing Vacuum Facility Backpressure Effets on the Performance of a Hall Thruster," *27th International Electric Propulsion Conference,* IEPC-01-045, Pasadena, CA, 15-19 October 2001

[47] Walker, M.L.R., "Effects of Facility Backpressure on the Performance and Plume of a Hall Thruster," *Doctoral Dissertation*, Aerospace Engineering, University of Michigan, 2005

[48] Walker, M.L.R., A.L. Victor, R.R. Hofer, and A.D. Gallimore, "Effect of Backpressure on Ion Current Density Measurements in Hall Thruster Plumes," Journal of Propulsion and Power, 21, 2005, pp. 408-415

[49] Rovey, J.L., M.L.R. Walker, and A.D. Gallimore, "Magnetically filtered Faraday probe for measuring the ion current density profile of a Hall thruster," Review of Scientific Instruments, 77, 013503 (2006); 10.1063/1.2149006

[50] Polzin, K.A., T.E. Markusic, B.J. Stanojev, and C. Marrese-Reading, "Integrated Liquid Bismuth Propellant Feed System," *42nd AIAA/ASME/SAE/ASEE Joint Propulsion Conference & Exhibit,* AIAA-2006-4636, Sacramento, CA, 9-12 July 2006

[51] Massey, D.R., L.B. King, and J.M. Makela, "Progress on the Development of a Direct Evaporation Bismuth Hall Thruster," *41st AIAA/ASME/SAE/ASEE Joint Propulsion Conferece & Exhibit,* AIAA-2005-4232, Tucson, AZ, 10-13 July 2005

[52] Kieckhafer, A.W., D.R. Massey, and L.B. King, "Performance and Active Thermal Control of 2-kW Hall Thruster with Segmented Electrodes," Journal of Propulsion and Power, 23, 2007, pp. 821-827

[53] Szabo, J., B. Pote, S. Paintal, M. Robin, A. Hillier, R.D. Branam, and R.E. Huffman, "Performance Evaluation of an Iodine-Vapor Hall Thruster," Journal of Propulsion and Power, 28, 2012, pp. 848-857

[54] Marrese-Reading, C., T.E. Markusic, K.A. Polzin, T. Knowles, and J. Mueller, "The Development of a Bismuth Feed Systen for the Very High Isp Thruster with Anode Layer VHITAL Program," *29th International Electric Propulsion Conference,* IEPC-2005-218, Princeton, NJ, 31 October - 4 November 2005

[55] Hopkins, M.A. and L.B. King, "Magnesium Hall Thruster with Active Thermal Mass Flow Control," Journal of Propulsion and Power, 30, 2014, pp. 637-644

[56] King, D., D. Tilley, R. Aadland, K. Nottingham, R. Smith, C. Roberts, V. Hruby, B. Pote, and J. Monheiser, "Development of the BPT Family of US-Designed Hall Current Thrusters for Commercial LEO and GEO Applications," *34th AIAA/ASME/SAE/ASEE Joint Propulsion Conference & Exhibit,* AIAA-1998-3338, Cleveland, OH,

[57] Haag, T.W., "Thrust stand for highpower electric propulsion devices," Review of Scientific Instruments, 65, 1991, pp. 1186-1191

[58] Xu, K.G. and M.L.R. Walker, "High-power, null-type, inverted pendulum thrust stand.," Review of Scientific Instruments, 80, 2009, pp.

[59] Sommerville, J.D., "Hall-Effect Thruster--Cathode Coupling," *Doctoral Dissertaion*, Mechanical Engineering-Engineering Mechanics, Michigan Technological University, 2009

[60] Raitses, Y., A. Smirnov, D. Staack, and N.J. Fisch, "Measurements of secondary electron emission effects in the Hall thruster discharge," Physics of Plasmas, 13, 014502 (2006); 10.1063/1.2162809

[61] Raitses, Y., D. Staack, M. Keidar, and N.J. Fisch, "Electron-wall interaction in Hall thrusters," Physics of Plasmas, 12, 057104 (2005); 10.1063/1.1891747

[62] Cohen-Zur, A., A. Fruchtman, J. Ashkenazy, and A. Gany, "Channel Length and Wall Recombination Effects in the Hall Thruster," *36th AIAA/ASME/SAE/ASEE Joint Propulsion Conference & Exhibit,* AIAA 2000-3654, Huntsville, AL, USA, 17-19 July, 2000

[63] Mikami, K., K. Komurasaki, and T. Fujiwara, "Optimization of Channel Configuration of Hall Thrusters," *23rd International Electric Propulsion Conference,* IEPC-95-33, Moscow, Russia, 1995

[64] Raitses, Y., D. Staack, L. Dorf, and N.J. Fisch, "Controlling Ion Acceleration Region in Hall Thrusters," *29th International Electric Propulsion Conference,* IEPC-2005-053, Princeton, NJ, USA, 31 Oct - 4 Nov, 2005

[65] Reid, B.M. and A.D. Gallimore, "Langmuir Probe Measurements in the Discharge Channel of a 6-kW Hall Thruster," *44th AIAA/ASME/SAE/ASEE Joint Propulsion Conference & Exhibit,* AIAA 2008-4920, Hartford, CT, USA, 21-23 Juy, 2008

[66] Reid, B.M. and A.D. Gallimore, "Plasma Potential Measurements in the Discharge Channel of a 6-kW Hall Thruster," *44th AIAA/ASME/SAE/ASEE Joint Propulsion Conference & Exhibit,* AIAA 2008-5185, Hartford, CT, USA, 21-23 July, 2008

[67] Wetzel, R.C., F.A. Baiocchi, T.R. Hayes, and R.S. Freund, "Absolute cross sections for electron-impact ionization of the rare-gas atoms by the fast-neutral-beam method," Physical Review A, 35, 1987, pp. 559-577

[68] Freund, R.S., R.C. Wetzel, R.J. Shul, and T.R. Hayes, "Cross-section measurements for electron-impact ionization of atoms," Physical Review A, 41, 1990, pp. 3575-3594

[69] Hayes, T.R., R.C. Wetzel, and R.S. Freund, "Absolute electron-impact-ionization cross-section of the halogen atoms," Physical Review A, 35, 1986, pp. 578-584

[70] Vainshtein, L.A., V.I. Ochkur, V.I. Rakhovskii, and A.M. Stepanov, "Absolute values of electron impact ionization cross sections for magnesium, calcium, strontium and barium.," Soviet Physics JETP, 34, 1972, pp. 271-275

[71] Hayashi, M., "Determination of electron-xenon total excitation cross-sections, from threshold to 100 eV, from experimental values of Townsend's," Journal of Physics D: Applied Physics, 16, 1982, pp. 581-589

[72] Boivin, R.F. and S.K. Srivastava, "Electron-impact ionization of Mg," Journal of Physics B: Atomic, Molecular and Optical Physics, 31, 1998, pp.

[73] Rapp, D. and P. Englander-Goldan, "Total Cross Sections for Ionization and Attachment in Gases by Electron Impact. I. Positive Ionization," Journal of Chemical Physics, 43, 1965, pp. 1464-1479

[74] Mikellides, I.G., I. Katz, R.R. Hofer, and D.M. Goebel, "Magnetic shielding of a laboratory Hall thruster. I. Theory and validation," Journal of Applied Physics, 115, 043303 (2014); 10.1063/1.4862313

[75] Hofer, R.R., D.M. Goebel, I.G. Mikellides, and I. Katz, "Magnetic shielding of a laboratory Hall thruster. II. Experiments," Journal of Applied Physics, 115, 043304 (2014); 10.1063/1.4862314
[76] Gombosi, T.I., *Gaskinetic theory*1994, New York, NY: Cambridge University Press.
[77] Zhou, Z.Q. and R.P. Burns, "Thermal desorption spectroscopy of magnesium from a chemical vapor deposited aluminum oxide surface," Applied Surface Science, 72, 1993, pp. 329-334
[78] Book, C.F. and M.L.R. Walker, "Effect of Anode Temperature on Hall Thruster Performance," Journal of Propulsion and Power, 26, 2010, pp. 1036-1044
[79] Lide, D.R., *CRC Handbook of Chemistry and Physics* 2004.